Diserinol Isophthalamide: A Novel Reagent for Complexation with Biomolecular Anions in Electrospray Ionization Mass Spectrometry

Madeline Schultz, Sarah L. Parker, Maleesha T. Fernando,‡ Miyuru M. Wellalage,‡ Daniel A. Thomas*

Department of Chemistry, University of Rhode Island, Kingston, RI 02881, USA

ABSTRACT: Transferring biomolecules from solution to vacuum facilitates a detailed analysis of molecular structure and dynamics by isolating molecules of interest from a complex environment. However, inherent in the ion desolvation process is the loss of solvent hydrogen bonding partners, which are critical for the stability of condensed-phase structure. Thus, transfer of ions to vacuum can favor structural rearrangement, especially near solvent-accessible charge sites, which tend to adopt intramolecular hydrogen bonding motifs in the absence of solvent. Complexation of monoalkylammonium moieties (e.g., lysine side chains) with crown ethers such as 18-crown-6 can disfavor structural rearrangement of protonated sites, but no equivalent ligand has been investigated for deprotonated groups. Herein we describe diserinol isophthalamide (DIP), a novel reagent for the gas-phase complexation of anionic moieties within biomolecules. Complexation is observed to the C-terminus or side chains of small model peptides GD, GE, GG, DF-OMe, VYV, YGGFL, and EYMPME in electrospray ionization mass spectrometry (ESI–MS) studies. In addition, complexation is observed with the phosphate and carboxylate moieities of phosphoserine and phosphotyrosine. DIP performs favorably in comparison to an existing anion recognition reagent, 1,1'-(1,2-phenylene)bis(3-phenylurea), that exhibits moderate carboxylate binding in organic solvent. This improved performance in ESI–MS experiments is attributed to reduced steric constraints to complexation with carboxylate groups of larger molecules. Overall, diserinol isophthalamide is an effective complexation reagent that can be applied in future work to study retention of solution-phase structure, investigate intrinsic molecular properties, and examine solvation effects.

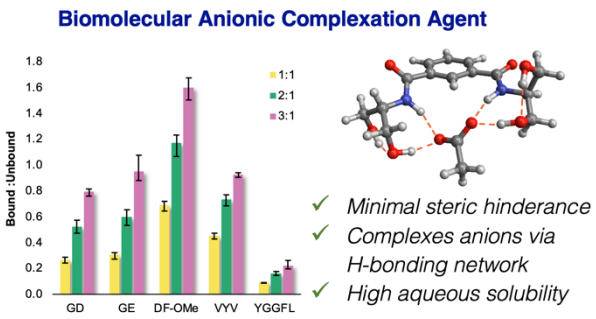

INTRODUCTION

Electrospray ionization (ESI) enables the transfer of biomolecular ions, such as proteins and peptides, from solution to the gas phase for characterization in vacuum.[1–3] In addition to primary sequence analysis via tandem mass spectrometry (MS),[4–7] the isolation of biomolecular ions in vacuum facilitates the investigation of secondary, tertiary, and even quaternary structure,[8,9] for example by the combination of mass spectrometry (MS) and ion mobility spectrometry (IMS)[10–16] or ion action spectroscopy.[17–19] These methods leverage the selectivity and control afforded by vacuum conditions to characterize well-defined and isolated structures, yielding information complementary to that obtained by traditional condensed-phase techniques that sample an ensemble of states. To yield further insight, experimental results often are compared to predictions from a variety of computational approaches including molecular dynamics simulations or electronic structure methods.[3,20–26]

As biomolecules are transferred from solution to vacuum via ESI, the loss of a solvation shell can favor structural rearrangement.[27] As intermolecular interactions are lost, intramolecular interactions often become the most energetically favored alternative, leading to conformational changes.[21,28–31] This phenomenon is especially prominent for charged functional groups, which form stabilizing ionic hydrogen bonds with solvent molecules.[27,32–34] Two approaches are typically employed to address any differences between condensed-phase and gas-phase structure. In one approach, model structural motifs such as short peptide sequences,[35–37] α-helices,[38–40] β-sheets,[27,41–43] and β-hairpins[28,29,44] are investigated in vacuum to reveal intrinsic structural properties. Characterization of solvent adduct species can then further unravel the contribution of intermolecular interactions.[14,27,37,45–50] Alternatively, native condensed-phase structures are kinetically trapped upon transfer to vacuum by carefully selecting instrument parameters to minimize energy deposition during the electrospray and vacuum transfer processes.[14,18,31,51,52] Experimental and theoretical investigations suggest that, for many model proteins, the condensed-phase structure is largely preserved under the appropriate conditions.[15,17,22,51] However, in other cases, side chain collapse occurs to accommodate intramolecular hydrogen bonding of desolvated charged moieties, resulting in structural perturbation.[22,53–55]

To modulate or disfavor structural rearrangement arising from intramolecular hydrogen bonding, charge recognition "microsolvation" reagents can be employed. For example, 18-crown-6 (18C6) has been used extensively to form noncovalent complexes with monoalkylammonium functional groups (e.g., protonated lysine and N-terminal residues).[33,56-65] Although the affinity of 18C6 for such sites is moderate in solution (estimated dissociation constant on the order of mM),[62,66] abundant adduct formation is observed in MS-based studies, suggesting that

complexation is favored during the electrospray process.[62] Notably, for biomolecules that adopt a well-defined conformation in solution, complexation occurs preferentially at solvent-accessible sites, yielding a correlation between condensed-phase structure and number of complexed 18C6 molecules. This relationship has been leveraged in selective noncovalent adduct protein probing (SNAPP) to quantify the influence of solvent conditions or primary sequence on protein structure.[33,34,57,61,63,64,67,68] In addition, IMS–MS and ultraviolet photodissociation (UVPD) MS experiments have indicated that complexation of proteins with 18C6 favors the retention of native-like structure upon transfer to vacuum.[32,33,69] IMS–MS has also been combined with tandem mass spectrometry experiments to elucidate the contribution of protonated lysine residues to structural rearrangement of ubiquitin during the ESI process.[70]

Although complexation with 18C6 has proven a valuable tool for the analysis of isolated biomolecular cations, no equivalent ligand has been developed for complexation with anionic functional groups such as carboxylate moieties. Design requirements for such a reagent include (1) high solubility in aqueous solution, (2) strong binding to anionic sites through multiple coordinated hydrogen-bond donors, and (3) minimal steric hindrance to complexation with biomolecular ions. Despite extensive efforts to develop reagents for the recognition of small anions in the condensed phase,[71-81] few molecules exist that fulfill these conditions. Herein we present N1,N3-bis[2-hydroxy-1-(hydroxymethyl)ethyl]-1,3-benzenedicarboxamide (Scheme 1, left), or diserinol isophthalamide (DIP), a suitable reagent for complexation to anionic moieties. We examine the complexation of this reagent with carboxylate groups in short peptides by ESI–MS and compare the results to those obtained with an established, commercially available, and relatively small anion recognition reagent, 1,1'-(1,2-phenylene)bis(3-phenylurea) (Scheme 1, right), or PBP.

Scheme 1. Anion Complexation reagents for MS studies

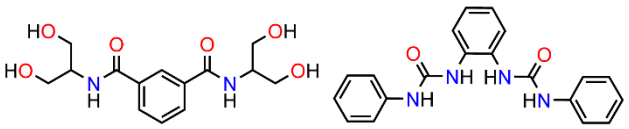

DIP PBP

EXPERIMENTAL

Synthesis of N1,N3-bis[2-hydroxy-1-(hydroxymethyl)ethyl]-1,3-benzenedicarboxamide

The synthesis was adapted from a procedure by Håland and Sydnes.[82] Dimethyl isophthalate, a white solid, and 2-amino-1,3-propanediol, a clear liquid, were purchased from Acros Organics (Fairlawn, NJ) and used without further purification. Dimethyl isophthalate (1 Eq, 0.64 mmol) and 2-Amino-1,3-propanediol (2.3 Eq. 1.47 mmol) were added to a 25 mL round-bottom flask equipped with a water-cooled condenser and slowly heated to 120–130° C (measured at the heating mantle-glass interface) while stirring for three hours to yield a sticky light-yellow gel. After three hours, the reaction was cooled to approximately 70° C, and a two-solvent recrystallization was performed; water was added dropwise until the reaction was clear, followed by the addition of methanol to cloudy, and finally water added to clear. The reaction mixture was cooled to room temperature and then placed into the freezer overnight. Vacuum filtration was performed, and the product was rinsed with cold methanol yielding a white, flakey solid (0.21 mmol, 49.3% yield). ^{1}H NMR (400 MHz, DMSO-d_6) δ 3.52 (m, 8H, CH-CH_2-OH), 3.94 (m, 2H, CH-CH_2-OH), 4.66 (t, 4H, OH), 7.54 (t, 1H, aryl), 7.97 (dd, 2H, NH), 8.07 (d, 2H, aryl) 8.30 (s, 1H, aryl). MS (ESI/quadrupole) *m*/*z*: $[M-H]^-$: 311.0.

Collection of Mass Spectra

Leucine Enkephalin (YGGFL) was purchased from Alfa Aesar (Fairlawn, NJ USA). Aspartame (DF-OMe), Valine-Tyrosine-Valine (VYV), Glycyl-L-aspartic acid (GD), O-Phospho-L-tyrosine (pY) and 1,1'-(1,2-phenylene)bis(3-phenylurea) (PBP) were purchased from Sigma-Aldrich (St. Louis, MO USA). Glycyl-L-glutamic Acid (GE), O-phospho-L-Phosphoserine (pS) and glycyl glycine (GG) were purchased from TCI (Portland, OR USA), and amidated YGGFL was purchased from Thermo Fisher Scientific (Fairlawn, NJ USA). Glu-Glu epitope tag (EYMPME) was purchased from Anaspec (Fremont, CA USA). All reagents were used as supplied. To prepare 1 mM solutions; PBP was dissolved in 90/10 MeOH/DMSO (v/v%); GE, GG, GF-OMe, pS, pY, EYMPME, and DIP were dissolved in H_2O; VYV was dissolved in MeOH; and YGGFL was dissolved in 80/20 H_2O/MeOH (v/v%). From 1 mM stock solutions, all final samples were then prepared in 80/20 H_2O/MeOH (v/v%) with 10 μM peptide and 10-30 μM complexation reagent, respectively, except for EYMPME, where a complexation reagent concentration of 60 μM was used. Mass spectra were collected in negative mode on a Shimazdu LCMS 2020 with an eluent flow of 80/20 H_2O/MeOH (v/v%) at 20 μL/min and an injection volume of 10 μL. All samples were run in triplicate.

Determination of Association Constants via NMR titration

The association constant of acetate ions, provided as a tetrabutylammonium acetate (TBAA), purchased from Sigma Aldrich (St. Louis, MO USA), to complexation reagents 1,1'-(1,2-phenylene)bis(3-phenylurea) and N1,N3-bis[2-hydroxy-1-(hydroxymethyl)ethyl]-1,3-benzenedicarboxamide was measured by NMR titration. The concentration of complexation agent was 10 mM in 99.5% DMSO-d_6 with 0.5% D_2O (v/v%) for all spectra collected, with varying acetate equivalence from 0 to 2.4 for 1,1'-(1,2-phenylene)bis(3-phenylurea) and 0 to 3.2 for N1,N3-bis[2-hydroxy-1-(hydroxymethyl)ethyl]-1,3-benzenedicarboxamide. All samples were collected in duplicate. Spectra were collected on a Bruker Avance III HD NMR Spectrometer (400 MHz). Association constants were calculated as previously detailed by Kadam *et al*.[81]

Electronic Structure Methods

Structural optimization of the complex between DIP or PBP and acetate was carried out using the Gaussian 16 software package with default convergence criteria.[83] The hybrid density functionals PBE0,[84,85] B3LYP,[86-88] and CAM-B3LYP[89] were employed in combination with the empirical dispersion correction developed by Grimme and co-workers with Becke-Johnson damping (D3BJ).[90,91] Structures were also optimized using the Møller-Plesset second-order perturbation method (MP2).[92] For all methods, the 6-311++G(d,p) Pople basis set was used.[93,94] Additional optimization was performed with the def2-TZVPP basis set of Ahlrichs and co-workers[95,96] in combination with the PBE0(D3BJ) density functional method.

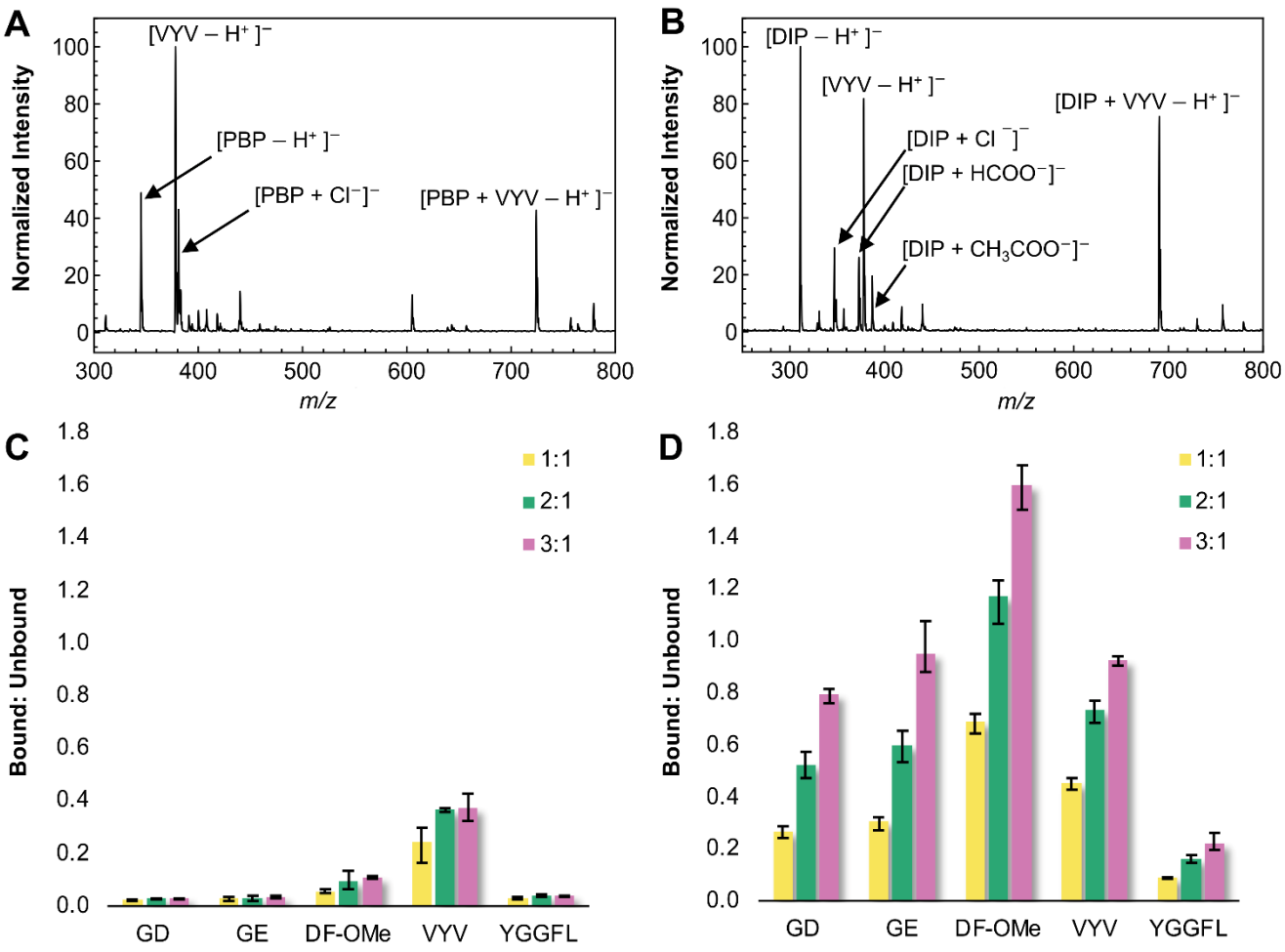

Figure 1. The ESI mass spectrum from solutions of 30 μM PBP (A) or DIP (B) and 10 μM VYV in 80/20 H_2O/MeOH (v/v%) are shown. Complexation to several peptides was examined for PBP (C) and DIP (D), and the ratio of the intensity of the bound complex to free peptide was calculated. Error bars show the minimum and maximum values from three samples.

RESULTS AND DISCUSSION

As discussed in the introduction, the ideal reagent for ESI–MS-based studies of biomolecules should be soluble in water, form a complex with anionic sites via hydrogen bond donors, and be small enough to avoid steric hindrance to complexation. In addition, commercial availability and/or facile synthesis are highly desirable. In this work, we have investigated the complexation between two candidate reagents and short anionic peptides (two to four residues) using ESI–MS. The first reagent, 1,1'-(1,2-phenylene)bis(3-phenylurea) (Scheme 1, right), or PBP, is commercially available, whereas the second, N1,N3-bis[2-hydroxy-1-(hydroxymethyl)ethyl]-1,3-benzenedicarboxamide (Scheme 1, left), or diserinol isophthalamide (DIP), is easily synthesized.

Peptide complexation of PBP and DIP

PBP, first synthesized in 1966,[97] was found by Brooks and coworkers to exhibit moderate association constants of ca. 10^3 M^{-1} with small carboxylate molecules in 99.5/0.5% (v/v) DMSO/H_2O solutions.[71] Further, a crystal structure of the complex with benzoate revealed the formation of four hydrogen bonds coordinating the two urea bridges to the acceptor carboxylate moiety. These results suggested PBP as a promising anion recognition reagent for MS experiments. However, PBP is poorly soluble in water and common polar organic solvents, except for dimethyl sulfoxide (DMSO), therefore limiting its applicability in aqueous studies of biomolecular structure.[98] Nevertheless, we were able to perform MS experiments by preparing a stock solution in DMSO and diluting to a final concentration of 10–30 μM in 80/20% (v/v) H_2O/MeOH (0.1% DMSO by volume) with a peptide concentration of 10 μM, yielding a reagent:peptide ratio ranging from 1:1 to 3:1. As a metric to assess and compare the extent of complexation, the observed intensity ratio between bound and unbound peptide anion was calculated for each sample.

In contrast to the moderate affinity for small carboxylates observed in DMSO, poor complexation of PBP with peptides was observed from aqueous solutions by ESI–MS (Figure 1c). Of the peptides tested (GD, GE, GG, DF-OMe, VYV and YGGFL), the most abundant complexation was observed for the 3:1 PBP:peptide samples of VYV (Figure 1a) and GG (Figures S1, S14), with bound:unbound ratios of 1:3 and 1:1.7 respectively. The complexation of GG is not ascribed to an exceptional affinity for PBP but rather is attributed to the low intensity of free anion, possibly arising from poor ionization efficiency or inefficient ion transfer through the front end of the instrument. Poor complexation was observed for all other

peptides (Figure 1c), indicating limited utility for PBP as an anion complexation reagent in MS experiments.

Because of the poor performance of PBP, an alternative complexation reagent, DIP (Scheme 1, left), was designed and synthesized. DIP comprises two serinol (2-amino-1,3-propanediol) moieties symmetrically linked via amide bonds to a rigid spacer based on isophthalic acid. This polar reagent is highly water-soluble and easily synthesized in a neat one-pot reaction. In addition, the six potential hydrogen bond donor sites may favorably coordinate with carboxylate moieties. In comparison to PBP, more abundant complexation is observed with all model peptides studied here (Figure 1c vs 1d). The degree of complexation was found to increase approximately linearly with increasing concentration ratio of reagent to peptide in solution, a trend which was not conclusively observed with PBP. For GD and GE, which possess two possible binding sites (both the C-terminus and the D or E side chain), simultaneous complexation at both charged sites was not observed, and the spectra were dominated by singly charged anions. This result is attributed to the proximity of the two charge sites, which may disfavor both formation of the doubly charged species and complexation with DIP. Interestingly, VYV and DF-OMe were observed to exhibit complexation with comparable or increased abundance to that of GD and GE despite having only one carboxylate site. Both peptides contain an aromatic side chain in proximity to the binding site, suggesting a possible contribution from aromatic stacking interactions between the peptide and DIP.[99] The abundance of DIP adducts with YGGFL was significantly lower than that of the other examined peptide sequences, which may be attributed in part to the strong binding of DIP to trifluoroacetate present in the sample (Figure S20). Additional investigation is required to elucidate the origin of this phenomenon.

In addition to complexation with peptide carboxylate moieties, significant adduction of DIP to background chloride and carboxylate ions was observed (Figure 1b, Figures S16–S21). Similar adduction to background cationic species, namely potassium, sodium, and ammonium, was previously reported for 18C6.[100] Furthermore, the deprotonated form of DIP (*m/z* 311) was the base peak in all spectra. The propensity for deprotonation of DIP is attributed to the multiple hydrogen bond donors in this reagent, which may form intramolecular hydrogen bonds that stabilize a deprotonated hydroxyl group. The abundance of $[DIP - H^+]^-$ is somewhat problematic, as it may lead to ionization suppression of the target peptides. Future reagent design that eliminates or minimizes this tendency for deprotonation, for example by replacing hydroxyl groups with amide or amine hydrogen bond donors, is therefore deserving of future investigation.

Multiple Site Complexation of DIP

To enable structural analysis of larger biomolecular ions, DIP complexation with multiple anionic sites is necessary. However, such multiple binding was not observed for GE and GD. Therefore, we expanded our substrate scope to determine the plausibility of concurrent multi-site complexation by DIP. As shown in Figure 2, DIP binding to phosphoserine (pS, Figure 2A), phosphotyrosine (pY, Figure 2B), and the peptide EYMPME (Figure 2C) was investigated. Because DIP is a non-specific anionic complexation agent, we expected possible complexation to both phosphate and carboxylate moieties of pS and pY. Both phosphorylated amino acids were observed to ionize rather weakly, and the spectra are dominated by the deprotonated DIP anion. In the case of pY (Figure 2A), the intensity of the doubly complexed, doubly deprotonated anion is approximately equal to that of the unbound, doubly deprotonated anion. The singly complexed, doubly deprotonated anion is also observed with roughly equal intensity. In contrast, predominant double complexation is observed for the doubly deprotonated pS anion (Figure 2B), with signal from the singly complexed, doubly deprotonated ion (*m/z* 247.6) extremely weak. The binding efficiency cannot be assessed for this species, as doubly deprotonated pS is found below the low-mass cutoff of the instrument. These results indicate that concurrent complexation can occur in certain species even at proximal binding sites. In this case, the different ionization properties and/or binding affinities of the phosphate groups appear to increase the propensity for double complexation over the somewhat analogous dicarboxylate peptides GD and GE.

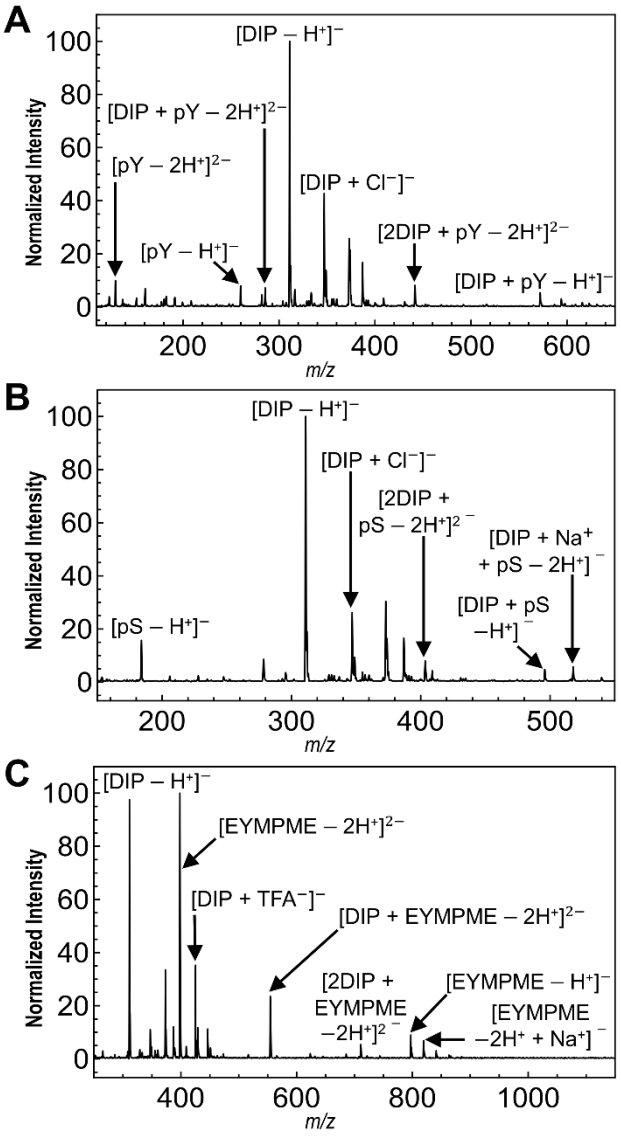

Figure 2. The ESI mass spectrum from solutions of 30 μM DIP: 10 μM pY (A), 30 μM DIP: 10 μM pS (B) and 60μM DIP: 10μM EYMPYE in 80/20 H_2O/MeOH (v/v%) are shown.

Complexation of DIP with the peptide EYMPYE was investigated to assess concurrent reagent complexation at remote carboxylate moieties, where any steric hinderance is expected to be reduced. As shown in Figure 2C, doubly deprotonated EYMPME is found as the base peak in the mass spectrum, and

the singly and doubly complexed peptides are observed at approximately 25% and 5% of base peak intensity, respectively. Surprisingly, no appreciable complexation to the singly deprotonated peptide is observed (*m/z* 1104), and further experimentation is required to understand this phenomenon. These results demonstrate that multiple concurrent binding of DIP reagents is possible, although additional work is needed to assess the limitations of this reagent.

NMR Titration Studies and Comparison with ESI–MS

Based on the ESI–MS experiments, we expected that the acetate binding constant of DIP in solution should be higher than that of PBP. To test this theory, host-guest NMR titrations were performed in DMSO with a small percentage of water added, standard conditions for the study of anion complexation reagents.[74,75,79,81] The association constants ($\log K_{ass}$) for binding to acetate, measured in DMSO-d_6 (0.5% D_2O), were found to be 3.88 M^{-1} and 2.39 M^{-1} for PBP and DIP, respectively. Measurement quality can be characterized by an average pooled standard deviation of 0.13 from the four-measurement series of PBP and DIP. The measured constant for PBP is in good agreement with previous studies in DMSO-d_6 (0.5% H_2O),[71,78,101]. Interestingly, the measured association constants are inverse to the complexation propensity observed by ESI–MS, with the binding significantly weaker for DIP than PBP. Notably, as discussed in the next section, these binding constants were obtained for acetate, which is much less susceptible to steric hindrance during reagent complexation than the peptide anions studied by ESI–MS.

Given the difference in solution conditions between the NMR titration and ESI–MS experiments, it is difficult to ascertain whether the favorable complexation of DIP observed in mass spectra is attributable to electrospray conditions or to some preferential binding in aqueous solvent. Unfortunately, NMR titration experiments under aqueous conditions are not feasible as carboxylates are strongly solvated, and therefore weakly complexed. Generally, binding affinities of anion recognition reagents decrease as the aqueous solvent component is increased, which suggests that the observed complexation of DIP occurs preferentially during the electrospray process. Similar to DIP, solution phase complexation between cationic primary amines and 18C6 is low compared to gas phase adduction.[64] This increased complexation is thereby attributed to the electrospray process. In the case of 18C6, experimental evidence indicates that charge sites of biomolecules bind to 18C6 on a shorter time scale than that for structural rearrangement, allowing for structural retention.[102] It is reasonable to expect similar complexation time scales for DIP during the electrospray process.

An alternate explanation for the abundance of peptide complexes with DIP in ESI–MS experiments may be complexation between the anionic form of the reagent (i.e., $[DIP - H^+]^-$) and neutral peptide species. To investigate whether the DIP anion undergoes such complexation, a control ESI–MS experiment was performed to examine potential complexation between DIP and amidated YGGFL, which lacks an anionic site. No complexation was observed (Figure S22), suggesting that the DIP anion does not bind strongly to neutral peptide species. We therefore expect that the observed complexes are formed between neutral reagent and anionic peptides.

Binding Motif of DIP and PBP from Electronic Structure Methods

To identify possible binding motifs of DIP and PBP with carboxylate moieties, structures for the complex between acetate and these reagents were optimized using electronic structure methods. Shown in Figure 3 are the low-energy structures for each complex obtained at the PBE0(D3BJ)/6-311++G(d, p) level of theory (**1**, **3**) and the MP2/6-311++G(d, p) level of theory (**2**, **4**). The local and global minimum-energy structure was found to be dependent on the method and level of theory employed, indicating the challenge of accurately predicting the structure and energetics in these systems. For acetate complexation with DIP (**1** and **2**, Figure 3), both methods predict the formation of four ionic hydrogen bonds between the anion and reagent, with an additional two intramolecular hydrogen bonds participating in an extended hydrogen bonding network. However, the PBE0(D3BJ) method predicts a nearly symmetric structure (**1**), with the two serinol moieties residing on opposite sides of the aromatic plane.

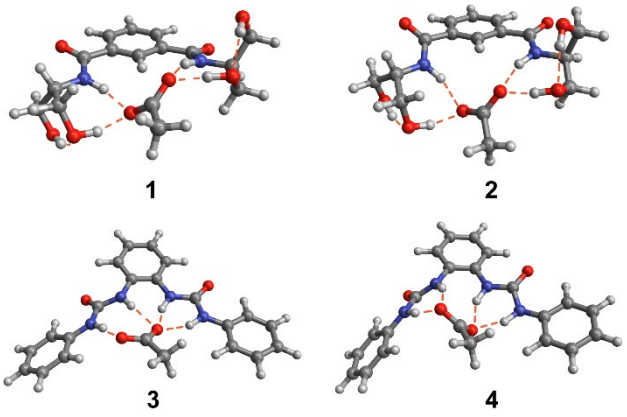

Figure 3. Computed low-energy structures for complexation of acetate with DIP (**1**, **2**) and PBP (**3**, **4**). Slight conformational differences are found at the PBE0(D3BJ)/6-311++G(d, p) level of theory (**1**, **3**) and the MP2/6-311++G(d, p) level of theory (**2**, **4**).

In contrast, the low-energy structure obtained with the MP2 method (**2**) shows both serinol moieties on the same side of the aromatic plane. This structure was found to be only slightly lower in energy (−0.4 kJ mol^{-1}) than structure **1** with the MP2 method. In contrast, structure **2** was not found as a local minimum with the PBE0(D3BJ) method. Optimization with additional hybrid functionals [CAM-B3LYP(D3BJ), B3LYP(D3BJ)] and an additional basis set [PBE0(D3BJ)/def2-TZVPP] yielded similar results to those obtained at the PBE0(D3BJ)/6-311++G(d, p) level of theory (i.e., structure **1**).

For the complex of acetate with PBP, optimization at the PBE0(D3BJ)/6-311++G(d, p) level of theory yielded an asymmetric structure featuring a single ionic hydrogen bond to one carboxylate oxygen and three ionic hydrogen bonds to the second carboxylate oxygen (**3**, Figure 3). Similar binding motifs were found using the B3LYP(D3BJ) and CAM-B3LYP(D3BJ) density functionals with the same basis set. Optimization at the MP2/6-311++G(d, p) level of theory yielded a more symmetric interaction of the acetate molecule with the two urea moieties and a much larger deviation from planarity (**4**, Figure 3). Notably, optimization at the PBE0(D3BJ)/def2-TZVPP level of theory yields a conformer similar to **4** rather than **3**.

Irrespective of the method-dependent differences in low-energy structures, the overall results reveal a stark contrast in the accessibility of the anion binding motif between DIP and PBP. In the DIP-acetate complex, structures **1** and **2** show that the

acetate methyl group extends away from the reagent, suggesting that the same binding motif should be accessible in larger molecules featuring a carboxylate moiety. In contrast, the binding pocket in the PBP-acetate complex (structures **3** and **4**) is closely flanked by the two phenyl moieties, which may impose substantial steric limitations on the binding of larger molecules. These results may partially account for the disparate performance of the two reagents in peptide complexation by ESI–MS.

CONCLUSIONS

The reagent diserinol isophthalamide, or DIP, exhibits favorable complexation to a series of small anionic peptide species, indicating its potential for anion binding in ESI–MS experiments. As compared to the established anion recognition reagent PBP, DIP was found to yield greater complexation in aqueous ESI-MS studies of peptides. However, NMR titration studies indicated that the binding affinity of DIP is significantly lower than that of PBP in DMSO solutions, suggesting that the DIP complexation occurs preferentially during the ESI process. The poor complexation of PBP in ESI–MS experiments may arise from steric constrains imposed by the flanking phenyl groups. Although complexation was observed across the model peptides examined, one considerable weakness of DIP is the propensity to readily deprotonate, yielding strong abundance of the anionic species in ESI–MS.

Future work will focus on structural modifications to DIP to better retain the neutral form while maintaining high solubility in aqueous media, strong hydrogen bonding, and a compact structure. In addition, spectroscopic studies will be useful to identify the binding motif of this reagent. Further investigation is also needed to assess the propensity of DIP for multiple concurrent complexation with biomolecular anions. Finally, studies are necessary to investigate the complexation of DIP with larger peptides and proteins and to explore possible complexation with phosphorylated peptides and nucleic acids. Overall, DIP provides a starting point for the development of anion recognition reagents to study the retention of biomolecular structure in vacuum and the examination of microsolvation effects.

ASSOCIATED CONTENT

Supporting Information

The Supporting Information is available free of charge on the ACS Publications website.

Supporting Information: ^{1}H NMR of DIP, ^{1}H NMR titrations for DIP and PBP; Figures showing normalized intensity of complexed species, uncomplexed reagents and free peptides and mass spectra for all peptides tested for both PBP and DIP

AUTHOR INFORMATION

Corresponding Author

* Daniel Thomas- Department of Chemistry, University of Rhode Island, Kingston, RI 02881, USA; Email: dathomas@uri.edu

Authors

‡These authors contributed equally.

Notes

The authors declare no competing financial interest.

ACKNOWLEDGMENT

We would like to graciously thank Dr. Ivo Leito from the University of Tartu Institute of Chemistry for assistance and guidance throughout the NMR titration studies. We thank the Fritz-Haber-Institut der Max-Planck-Gesellschaft for providing computational resources. This work was supported by startup funding from the University of Rhode Island and NSF grant CHE-2212926.

REFERENCES

(1) Fenn, J.; Mann, M.; Meng, C.; Wong, S.; Whitehouse, C. Electrospray Ionization for Mass Spectrometry of Large Biomolecules. *Science* **1989**, *246* (4926), 64–71. https://doi.org/10.1126/science.2675315.

(2) Kebarle, P.; Verkcerk, U. H. Electrospray: From Ions in Solution to Ions in the Gas Phase, What We Know Now. *Mass Spectrom. Rev.* **2009**, *28* (6), 898–917. https://doi.org/10.1002/mas.20247.

(3) Konermann, L.; Ahadi, E.; D. Rodriguez, A.; Vahidi, S. Unraveling the Mechanism of Electrospray Ionization. *Anal. Chem.* **2012**, *85* (1), 2–9. https://doi.org/10.1021/ac302789c.

(4) Schürch, S. Characterization of Nucleic Acids by Tandem Mass Spectrometry - The Second Decade (2004–2013): From DNA to RNA and Modified Sequences. *Mass Spectrom. Rev.* **2016**, *35* (4), 483–523. https://doi.org/https://doi.org/10.1002/mas.21442.

(5) L. Tabb, D.; Vega-Montoto, L.; A. Rudnick, P.; Mulayath Variyath, A.; L. Ham, A.-J.; M. Bunk, D.; E. Kilpatrick, L.; D. Billheimer, D.; K. Blackman, R.; L. Cardasis, H.; A. Carr, S.; R. Clauser, K.; D. Jaffe, J.; A. Kowalski, K.; A. Neubert, T.; E. Regnier, F.; Schilling, B.; J. Tegeler, T.; Wang, M.; Wang, P.; R. Whiteaker, J.; J. Zimmerman, L.; J. Fisher, S.; W. Gibson, B.; R. Kinsinger, C.; Mesri, M.; Rodriguez, H.; E. Stein, S.; Tempst, P.; G. Paulovich, A.; C. Liebler, D.; Spiegelman, C. Repeatability and Reproducibility in Proteomic Identifications by Liquid Chromatography−Tandem Mass Spectrometry. *J. Proteome Res.* **2009**, *9* (2), 761–776. https://doi.org/10.1021/pr9006365.

(6) Sleno, L.; Volmer, D. A. Ion Activation Methods for Tandem Mass Spectrometry. *J. Mass Spectrom.* **2004**, *39* (10), 1091–1112. https://doi.org/10.1002/jms.703.

(7) Hernandez, P.; Müller, M.; Appel, R. D. Automated Protein Identification by Tandem Mass Spectrumetry: Issues and Strategies. *Mass Spectrom. Rev.* **2006**, *25* (2), 235–254. https://doi.org/10.1002/mas.20068.

(8) J. Morrison, L.; S. Brodbelt, J. 193 Nm Ultraviolet Photodissociation Mass Spectrometry of Tetrameric Protein Complexes Provides Insight into Quaternary and Secondary Protein Topology. *J. Am. Chem. Soc.* **2016**, *138* (34), 10849–10859. https://doi.org/10.1021/jacs.6b03905.

(9) Benesch, J. L. P.; Aquilina, J. A.; Ruotolo, B. T.; Sobott, F.; Robinson, C. V. Tandem Mass Spectrometry Reveals the Quaternary Organization of Macromolecular Assemblies. *Chem. Biol.* **2006**, *13* (6), 597–605. https://doi.org/10.1016/j.chembiol.2006.04.006.

(10) Wang, S. C.; Politis, A.; Di Bartolo, N.; Bavro, V. N.; Tucker, S. J.; Booth, P. J.; Barrera, N. P.; Robinson, C. V. Ion Mobility Mass Spectrometry of Two Tetrameric Membrane Protein Complexes Reveals Compact Structures and Differences in Stability and Packing. *J. Am. Chem. Soc.* **2010**, *132* (44), 15468–15470. https://doi.org/10.1021/ja104312e.

(11) Ruotolo, B. T.; Benesch, J. L. P.; Sandercock, A. M.; Hyung, S. J.; Robinson, C. V. Ion Mobility-Mass Spectrometry Analysis of Large Protein Complexes. *Nat. Protoc.* **2008**, *3* (7), 1139–1152. https://doi.org/10.1038/nprot.2008.78.

(12) McCabe, J. W.; Hebert, M. J.; Shirzadeh, M.; Mallis, C. S.; Denton, J. K.; Walker, T. E.; Russell, D. H. The IMS Paradox: A Perspective on Structural Ion Mobility-Mass Spectrometry. *Mass Spectrom. Rev.* **2021**, *40* (3), 280–305. https://doi.org/10.1002/mas.21642.

(13) Theisen, A.; Yan, B.; M. Brown, J.; Morris, M.; Bellina, B.; E. Barran, P. Use of Ultraviolet Photodissociation Coupled with Ion Mobility Mass Spectrometry To Determine Structure and Sequence from Drift Time Selected Peptides and Proteins. *Anal. Chem.* **2016**, *88* (20), 9964–9971. https://doi.org/10.1021/acs.analchem.6b01705.

(14) A. Servage, K.; A. Silveira, J.; L. Fort, K.; H. Russell, D. Cryogenic Ion Mobility-Mass Spectrometry: Tracking Ion Structure from Solution to the Gas Phase. *Acc. Chem. Res.* **2016**, *49* (7), 1421–1428. https://doi.org/10.1021/acs.accounts.6b00177.

(15) Wyttenbach, T.; Bowers, M. T. Structural Stability from Solution to the Gas Phase: Native Solution Structure of Ubiquitin Survives Analysis in a Solvent-Free Ion Mobility-Mass Spectrometry Environment. *J. Phys. Chem. B* **2011**, *115* (42), 12266–12275. https://doi.org/10.1021/jp206867a.

(16) Bohrer, B. C.; Merenbloom, S. I.; Koeniger, S. L.; Hilderbrand, A. E.; Clemmer, D. E. Biomolecule Analysis by Ion Mobility Spectrometry. *Annu. Rev. Anal. Chem.* **2008**, *1* (1), 293–327. https://doi.org/10.1146/annurev.anchem.1.031207.113001.

(17) Seo, J.; Hoffmann, W.; Warnke, S.; Bowers, M. T.; Pagel, K.; von Helden, G. Retention of Native Protein Structures in the Absence of Solvent: A Coupled Ion Mobility and Spectroscopic Study. *Angew. Chemie - Int. Ed.* **2016**, *55* (45), 14173–14176. https://doi.org/10.1002/anie.201606029.

(18) Kamrath, M. Z.; R. Rizzo, T. Combining Ion Mobility and Cryogenic Spectroscopy for Structural and Analytical Studies of Biomolecular Ions. *Acc. Chem. Res.* **2018**, *51* (6), 1487–1495. https://doi.org/10.1021/acs.accounts.8b00133.

(19) Rijs, A. M.; Oomens, J. IR Spectroscopic Techniques to Study Isolated Biomolecules BT - Gas-Phase IR Spectroscopy and Structure of Biological Molecules; Rijs, A. M., Oomens, J., Eds.; Springer International Publishing: Cham, 2015; pp 1–42. https://doi.org/10.1007/128_2014_621.

(20) Schubert, F.; Rossi, M.; Baldauf, C.; Pagel, K.; Warnke, S.; Von Helden, G.; Filsinger, F.; Kupser, P.; Meijer, G.; Salwiczek, M.; Koksch, B.; Scheffler, M.; Blum, V. Exploring the Conformational Preferences of 20-Residue Peptides in Isolation: Ac-Ala19-Lys + H+vs. Ac-Lys-Ala19 + H+ and the Current Reach of DFT. *Phys. Chem. Chem. Phys.* **2015**, *17* (11), 7373–7385. https://doi.org/10.1039/c4cp05541a.

(21) Baldauf, C.; Rossi, M. Going Clean: Structure and Dynamics of Peptides in the Gas Phase and Paths to Solvation. *J. Phys. Condens. Matter* **2015**, *27* (49). https://doi.org/10.1088/0953-8984/27/49/493002.

(22) Bakhtiari, M.; Konermann, L. Protein Ions Generated by Native Electrospray Ionization: Comparison of Gas Phase, Solution, and Crystal Structures. *J. Phys. Chem. B* **2019**, *123* (8), 1784–1796. https://doi.org/10.1021/acs.jpcb.8b12173.

(23) Konermann, L. Molecular Dynamics Simulations on Gas-Phase Proteins with Mobile Protons: Inclusion of All-Atom Charge Solvation. *J. Phys. Chem. B* **2017**, *121* (34), 8102–8112. https://doi.org/10.1021/acs.jpcb.7b05703.

(24) Vahidi, S.; B. Stocks, B.; Konermann, L. Partially Disordered Proteins Studied by Ion Mobility-Mass Spectrometry: Implications for the Preservation of Solution Phase Structure in the Gas Phase. *Anal. Chem.* **2013**, *85* (21), 10471–10478. https://doi.org/10.1021/ac402490r.

(25) Luan, M.; Hou, Z.; Huang, G. Suppression of Protein Structural Perturbations in Native Electrospray Ionization during the Final Evaporation Stages Revealed by Molecular Dynamics Simulations. *J. Phys. Chem. B* **2022**, *126* (1), 144–150. https://doi.org/10.1021/acs.jpcb.1c09130.

(26) Bleiholder, C.; Liu, F. C. Structure Relaxation Approximation (SRA) for Elucidation of Protein Structures from Ion Mobility Measurements. *J. Phys. Chem. B* **2019**, *123* (13), 2756–2769. https://doi.org/10.1021/acs.jpcb.8b11818.

(27) S., N. N.; R., R. T.; V., B. O. Interplay of Intra- and Intermolecular H-Bonding in a Progressively Solvated Macrocyclic Peptide. *Science* **2012**, *336* (6079), 320–323. https://doi.org/10.1126/science.1218709.

(28) DeBlase, A. F.; Harrilal, C. P.; Lawler, J. T.; Burke, N. L.; McLuckey, S. A.; Zwier, T. S. Conformation-Specific Infrared and Ultraviolet Spectroscopy of Cold [YAPAA+H]+ and [YGPAA+H]+ Ions: A Stereochemical "Twist" on the β-Hairpin Turn. *J. Am. Chem. Soc.* **2017**, *139* (15), 5481–5493. https://doi.org/10.1021/jacs.7b01315.

(29) L. Burke, N.; F. DeBlase, A.; G. Redwine, J.; R. Hopkins, J.; A. McLuckey, S.; S. Zwier, T. Gas-Phase Folding of a Prototypical Protonated Pentapeptide: Spectroscopic Evidence for Formation of a Charge-Stabilized β-Hairpin. *J. Am. Chem. Soc.* **2016**, *138* (8), 2849–2857. https://doi.org/10.1021/jacs.6b00093.

(30) Voronina, L.; Masson, A.; Kamrath, M.; Schubert, F.; Clemmer, D.; Baldauf, C.; Rizzo, T. Conformations of Prolyl-Peptide Bonds in the Bradykinin 1-5 Fragment in Solution and in the Gas Phase. *J. Am. Chem. Soc.* **2016**, *138* (29), 9224–9233. https://doi.org/10.1021/jacs.6b04550.

(31) Voronina, L.; Rizzo, T. R. Spectroscopic Studies of Kinetically Trapped Conformations in the Gas Phase: The Case of Triply Protonated Bradykinin. *Phys. Chem. Chem. Phys.* **2015**, *17* (39), 25828–25836. https://doi.org/10.1039/c5cp01651g.

(32) Warnke, S.; Helden, G. Von; Pagel, K. Protein Structure in the Gas Phase: The Influence of Side-Chain Microsolvation. *J. Am. Chem. Soc.* **2013**, *135*, 1177–1180.

(33) Bonner, J. G.; Hendricks, N. G.; Julian, R. R. Structural Effects of Solvation by 18-Crown-6 on Gaseous Peptides and TrpCage after Electrospray Ionization. *J. Am. Soc. Mass Spectrom.* **2016**, *27* (10), 1661–1669. https://doi.org/10.1007/s13361-016-1456-3.

(34) Silzel, J. W.; Murphree, T. A.; Paranji, R. K.; Guttman, M. M.; Julian, R. R. Probing the Stability of Proline Cis/Trans Isomers in the Gas Phase with Ultraviolet Photodissociation. *J. Am. Soc. Mass Spectrom.* **2020**, *31* (9), 1974–1980. https://doi.org/10.1021/jasms.0c00242.

(35) Voss, J. M.; Fischer, K. C.; Garand, E. Revealing the Structure of Isolated Peptides: IR-IR Predissociation Spectroscopy of Protonated Triglycine Isomers. *J. Mol. Spectrosc.* **2018**, *347*, 28–34. https://doi.org/10.1016/j.jms.2018.03.006.

(36) Sherman, S. L.; Fischer, K. C.; Garand, E. Conformational Changes Induced by Methyl Side-Chains in Protonated Tripeptides Containing Glycine and Alanine Residues. *J. Phys. Chem. A* **2022**. https://doi.org/10.1021/acs.jpca.2c02584.

(37) Garand, E. Spectroscopy of Reactive Complexes and Solvated Clusters: A Bottom-Up Approach Using Cryogenic Ion Traps. *J. Phys. Chem. A* **2018**, *122* (32), 6479–6490. https://doi.org/10.1021/acs.jpca.8b05712.

(38) Hoffmann, W.; Marianski, M.; Warnke, S.; Seo, J.; Baldauf, C.; Von Helden, G.; Pagel, K. Assessing the Stability of Alanine-Based Helices by Conformer-Selective IR Spectroscopy. *Phys. Chem. Chem. Phys.* **2016**, *18* (29), 19950–19954. https://doi.org/10.1039/c6cp03827a.

(39) Jarrold, M. F. Helices and Sheets in Vacuo. *Phys. Chem. Chem. Phys.* **2007**, *9* (14), 1659–1671. https://doi.org/10.1039/b612615d.

(40) Stearns, J. A.; Boyarkin, O. V; Rizzo, T. R. Spectroscopic Signatures of Gas-Phase Helices : Ac-Phe- (Ala) 5 -Lys-H + And. *J. Am. Chem. Soc.* **2007**, *129* (45), 13820–13821.

(41) Nagornova, N. S.; Rlzzo, T. R.; Boyarkln, O. V. Highly Resolved Spectra of Gas-Phase Gramicidin S: A Benchmark for Peptide Structure Calculations. *J. Am. Chem. Soc.* **2010**, *132* (12), 4040–4041. https://doi.org/10.1021/ja910118j.

(42) Joshi, K.; Semrouni, D.; Ohanessian, G.; Clavaguéra, C. Structures and IR Spectra of the Gramicidin s Peptide: Pushing the Quest for Low-Energy Conformations. *J. Phys. Chem. B* **2012**, *116* (1), 483–490. https://doi.org/10.1021/jp207102v.

(43) Kupser, P.; Pagel, K.; Oomens, J.; Polfer, N.; Koksch, B.; Meijer, G.; Von Helden, G. Amide-I and -II Vibrations of the Cyclic β-Sheet Model Peptide Gramicidin S in the Gas Phase. *J. Am. Chem. Soc.* **2010**, *132* (6), 2085–2093. https://doi.org/10.1021/ja909842j.

(44) Kölbel, K.; Warnke, S.; Seo, J.; von Helden, G.; Moretti, R.; Meiler, J.; Pagel, K.; Sinz, A. Conformational Shift of a β-Hairpin Peptide upon Complex Formation with an Oligo-Proline Peptide Studied by Mass Spectrometry. *ChemistrySelect* **2016**, *1* (13), 3651–3656. https://doi.org/10.1002/slct.201600934.

(45) Fischer, K. C.; Sherman, S. L.; Voss, J. M.; Zhou, J.; Garand, E. Microsolvation Structures of Protonated Glycine and l -Alanine. *J. Phys. Chem. A* **2019**, *123* (15), 3355–3366. https://doi.org/10.1021/acs.jpca.9b01578.

(46) Voss, J. M.; Fischer, K. C.; Garand, E. Accessing the Vibrational Signatures of Amino Acid Ions Embedded in Water

Clusters. *J. Phys. Chem. Lett.* **2018**, *9* (9), 2246–2250. https://doi.org/10.1021/acs.jpclett.8b00738.

(47) Fischer, K. C.; Voss, J. M.; Zhou, J.; Garand, E. Probing Solvation-Induced Structural Changes in Conformationally Flexible Peptides: IR Spectroscopy of Gly3H+·(H2O). *J. Phys. Chem. A* **2018**, *122* (41), 8213–8221. https://doi.org/10.1021/acs.jpca.8b07546.

(48) Saparbaev, E.; Aladinskaia, V.; Zviagin, A.; Boyarkin, O. V. Microhydration of Biomolecules: Revealing the Native Structures by Cold Ion IR Spectroscopy. *J. Phys. Chem. Lett.* **2021**, *12* (2), 907–911. https://doi.org/10.1021/acs.jpclett.0c03678.

(49) Sherman, S. L.; Nickson, K. A.; Garand, E. Comment on "Microhydration of Biomolecules: Revealing the Native Structures by Cold Ion IR Spectroscopy." *J. Phys. Chem. Lett.* **2022**, *13* (8), 2046–2050. https://doi.org/10.1021/acs.jpclett.1c02211.

(50) Moghaddam, M. B.; Fridgen, T. D. IRMPD Spectroscopic Study of Microsolvated [Na(GlyAla)]+ and [Ca(GlyAla-H)]+ and the Blue Shifting of the Hydrogen-Bonded Amide Stretch with Each Water Addition. *J. Phys. Chem. B* **2013**, *117* (20), 6157–6164. https://doi.org/10.1021/jp402217g.

(51) Raab, S. A.; El-Baba, T. J.; Laganowsky, A.; Russell, D. H.; Valentine, S. J.; Clemmer, D. E. Protons Are Fast and Smart; Proteins Are Slow and Dumb: On the Relationship of Electrospray Ionization Charge States and Conformations. *J. Am. Soc. Mass Spectrom.* **2021**, *32* (7), 1553–1561. https://doi.org/10.1021/jasms.1c00100.

(52) Silveira, J. A.; Fort, K. L.; Kim, D.; Servage, K. A.; Pierson, N. A.; Clemmer, D. E.; Russell, D. H. From Solution to the Gas Phase: Stepwise Dehydration and Kinetic Trapping of Substance p Reveals the Origin of Peptide Conformations. *J. Am. Chem. Soc.* **2013**, *135* (51), 19147–19153. https://doi.org/10.1021/ja4114193.

(53) Steinberg, M. Z.; Elber, R.; McLafferty, F. W.; Gerber, R. B.; Breuker, K. Early Structural Evolution of Native Cytochrome c after Solvent Removal. *ChemBioChem* **2008**, *9* (15), 2417–2423. https://doi.org/10.1002/cbic.200800167.

(54) Rolland, A. D.; Biberic, L. S.; Prell, J. S. Investigation of Charge-State-Dependent Compaction of Protein Ions with Native Ion Mobility-Mass Spectrometry and Theory. *J. Am. Soc. Mass Spectrom.* **2022**, *33* (2), 369–381. https://doi.org/10.1021/jasms.1c00351.

(55) Rolland, A. D.; Prell, J. S. Computational Insights into Compaction of Gas-Phase Protein and Protein Complex Ions in Native Ion Mobility-Mass Spectrometry. *TrAC - Trends Anal. Chem.* **2019**, *116*, 282–291. https://doi.org/10.1016/j.trac.2019.04.023.

(56) McNary, C. P.; Nei, Y. W.; Maitre, P.; Rodgers, M. T.; Armentrout, P. B. Infrared Multiple Photon Dissociation Action Spectroscopy of Protonated Glycine, Histidine, Lysine, and Arginine Complexed with 18-Crown-6 Ether. *Phys. Chem. Chem. Phys.* **2019**, *21* (23), 12625–12639. https://doi.org/10.1039/c9cp02265a.

(57) Liu, Z.; Cheng, S.; Gallie, D. R.; Julian, R. R. Exploring the Mechanism of Selective Noncovalent Adduct Protein Probing Mass Spectrometry Utilizing Site-Directed Mutagenesis to Examine Ubiquitin. *Anal. Chem.* **2008**, *80* (10), 3846–3852. https://doi.org/10.1021/ac800176u.

(58) González Flórez, A. I.; Ahn, D. S.; Gewinner, S.; Schöllkopf, W.; Von Helden, G. IR Spectroscopy of Protonated Leu-Enkephalin and Its 18-Crown-6 Complex Embedded in Helium Droplets. *Phys. Chem. Chem. Phys.* **2015**, *17* (34), 21902–21911. https://doi.org/10.1039/c5cp02172c.

(59) Chen, Y.; Rodgers, M. T. Structural and Energetic Effects in the Molecular Recognition of Acetylated Amino Acids by 18-Crown-6. *J. Am. Soc. Mass Spectrom.* **2012**, *23* (11), 2020–2030. https://doi.org/10.1007/s13361-012-0466-z.

(60) Ko, J. Y.; Heo, S. W.; Lee, J. H.; Oh, H. Bin; Kim, H.; Kim, H. I. Host-Guest Chemistry in the Gas Phase: Complex Formation with 18-Crown-6 Enhances Helicity of Alanine-Based Peptides. *J. Phys. Chem. A* **2011**, *115* (49), 14215–14220. https://doi.org/10.1021/jp208045a.

(61) Ly, T.; Julian, R. R. Using ESI-MS to Probe Protein Structure by Site-Specific Noncovalent Attachment of 18-Crown-6. *J. Am. Soc. Mass Spectrom.* **2006**, *17* (9), 1209–1215. https://doi.org/10.1016/j.jasms.2006.05.007.

(62) Julian, R. R.; Beauchamp, J. L. Site Specific Sequestering and Stabilization of Charge in Peptides by Supramolecular Adduct Formation with 18-Crown-6 Ether by Way of Electrospray Ionization. *Int. J. Mass Spectrom.* **2001**, *210–211*, 613–623. https://doi.org/10.1016/S1387-3806(01)00431-6.

(63) Tao, Y.; Julian, R. R. Investigation of Peptide Microsolvation in the Gas Phase by Radical Directed Dissociation Mass Spectrometry. *Int. J. Mass Spectrom.* **2016**, *409*, 81–86. https://doi.org/10.1016/j.ijms.2016.10.001.

(64) Tao, Y.; Julian, R. R. Factors That Influence Competitive Intermolecular Solvation of Protonated Groups in Peptides and Proteins in the Gas Phase. *J. Am. Soc. Mass Spectrom.* **2013**, *24* (11), 1634–1640. https://doi.org/10.1007/s13361-013-0684-z.

(65) Stedwell, C. N.; Galindo, J. F.; Gulyuz, K.; Roitberg, A. E.; Polfer, N. C. Crown Complexation of Protonated Amino Acids: Influence on IRMPD Spectra. *J. Phys. Chem. A* **2013**, *117* (6), 1181–1188. https://doi.org/10.1021/jp305263b.

(66) Buschmann, H. J.; Schollmeyer, E.; Mutihac, L. Complexation of the Ammonium Ion by 18-Crown-6 in Different Solvents and by Noncyclic Ligands, Crown Ethers and Cryptands in Methanol. *Supramol. Sci.* **1998**, *5* (1–2), 139–142. https://doi.org/10.1016/S0968-5677(98)80005-9.

(67) Moore, B. N.; Hamdy, O.; Julian, R. R. Protein Structure Evolution in Liquid DESI as Revealed by Selective Noncovalent Adduct Protein Probing. *Int. J. Mass Spectrom.* **2012**, *330–332*, 220–225. https://doi.org/10.1016/j.ijms.2012.08.013.

(68) Ly, T.; Julian, R. R. Protein-Metal Interactions of Calmodulin and α-Synuclein Monitored by Selective Noncovalent Adduct Protein Probing Mass Spectrometry. *J. Am. Soc. Mass Spectrom.* **2008**, *19* (11), 1663–1672. https://doi.org/10.1016/j.jasms.2008.07.006.

(69) Zhou, L.; Liu, Z.; Guo, Y.; Liu, S.; Zhao, H.; Zhao, S.; Xiao, C.; Feng, S.; Yang, X.; Wang, F. Ultraviolet Photodissociation Reveals the Molecular Mechanism of Crown Ether Microsolvation Effect on the Gas-Phase Native-like Protein Structure. *J. Am. Chem. Soc.* **2022**. https://doi.org/10.1021/jacs.2c11210.

(70) Göth, M.; Lermyte, F.; Schmitt, X. J.; Warnke, S.; Von Helden, G.; Sobott, F.; Pagel, K. Gas-Phase Microsolvation of Ubiquitin: Investigation of Crown Ether Complexation Sites Using Ion Mobility-Mass Spectrometry. *Analyst* **2016**, *141* (19), 5502–5510. https://doi.org/10.1039/c6an01377e.

(71) Brooks, S. J.; Gale, P. A.; Light, M. E. Carboxylate Complexation by 1,1′-(1,2-Phenylene)Bis(3-Phenylurea) in Solution and the Solid State. *Chem. Commun.* **2005**, No. 37, 4696–4698. https://doi.org/10.1039/b508144k.

(72) Busschaert, N.; Caltagirone, C.; Van Rossom, W.; Gale, P. A. Applications of Supramolecular Anion Recognition. *Chem. Rev.* **2015**, *115* (15), 8038–8155. https://doi.org/10.1021/acs.chemrev.5b00099.

(73) Mammoliti, O.; Allasia, S.; Dixon, S.; Kilburn, J. D. Synthesis and Anion-Binding Properties of New Disulfonamide-Based Receptors. *Tetrahedron* **2009**, *65* (11), 2184–2195. https://doi.org/10.1016/j.tet.2009.01.070.

(74) Hiscock, J. R.; Caltagirone, C.; Light, M. E.; Hursthouse, M. B.; Gale, P. A. Fluorescent Carbazolylurea Anion Receptors. *Org. Biomol. Chem.* **2009**, *7* (9), 1781–1783. https://doi.org/10.1039/b900178f.

(75) Niedbała, P.; Majdecki, M.; Da¸browa, K.; Jurczak, J. Selective Carboxylate Recognition Using Urea-Functionalized Unclosed Cryptands: Mild Synthesis and Complexation Studies. *J. Org. Chem.* **2020**, *85* (7), 5058–5064. https://doi.org/10.1021/acs.joc.9b03082.

(76) Blažek Bregović, V.; Basarić, N.; Mlinarić-Majerski, K. Anion Binding with Urea and Thiourea Derivatives. *Coord. Chem. Rev.* **2015**, *295*, 80–124. https://doi.org/10.1016/j.ccr.2015.03.011.

(77) Hamann, B. C.; Branda, N. R.; Rebek, J. Multipoint Recognition of Carboxylates by Neutral Hosts in Non-Polar Solvents. *Tetrahedron Lett.* **1993**, *34* (43), 6837–6840. https://doi.org/https://doi.org/10.1016/S0040-4039(00)91808-2.

(78) Dydio, P.; Lichosyt, D.; Jurczak, J. Amide- and Urea-Functionalized Pyrroles and Benzopyrroles as Synthetic, Neutral Anion Receptors. *Chem. Soc. Rev.* **2011**, *40* (5), 2971–2985. https://doi.org/10.1039/c1cs15006e.

(79) Chmielewski, M. J.; Charon, M.; Jurczak, J. 1,8-Diamino-3,6-Dichlorocarbazole: A Promising Building Block for Anion Receptors. *Org. Lett.* **2004**, *6* (20), 3501–3504. https://doi.org/10.1021/ol048661e.

(80) Katayev, E. A.; Boev, N. V.; Myshkovskaya, E.; Khrustalev, V. N.; Ustynyuk, Y. A. Expanding Sapphyrin: Towards Selective Phosphate Binding. *Chem. - A Eur. J.* **2008**, *14* (29), 9065–9073. https://doi.org/10.1002/chem.200800860.

(81) Kadam, S. A.; Martin, K.; Haav, K.; Toom, L.; Mayeux, C.; Pung, A.; Gale, P. A.; Hiscock, J. R.; Brooks, S. J.; Kirby, I. L.; Busschaert, N.; Leito, I. Towards the Discrimination of Carboxylates by Hydrogen-Bond Donor Anion Receptors. *Chem. – A Eur. J.* **2015**, *21* (13), 5145–5160. https://doi.org/https://doi.org/10.1002/chem.201405858.

(82) Håland, T.; Sydnes, L. K. Formation of N,O-Acetalsin the Production of x-Ray Contrast Agents. *Org. Process Res. Dev.* **2014**, *18* (10), 1181–1190. https://doi.org/10.1021/op500177w.

(83) Frisch, M. J.; Trucks, G. W.; Schlegel, H. B.; Scuseria, G. E.; Robb, M. A.; Cheeseman, J. R.; Scalmani, G.; Barone, V.; Petersson, G. A.; Nakatsuji, H.; Li, X.; Caricato, M.; Marenich, A. V; Bloino, J.; Janesko, B. G.; Gomperts, R.; Mennucci, B.; Hratchian, H. P.; Ortiz, J. V; Izmaylov, A. F.; Sonnenberg, J. L.; Williams; Ding, F.; Lipparini, F.; Egidi, F.; Goings, J.; Peng, B.; Petrone, A.; Henderson, T.; Ranasinghe, D.; Zakrzewski, V. G.; Gao, J.; Rega, N.; Zheng, G.; Liang, W.; Hada, M.; Ehara, M.; Toyota, K.; Fukuda, R.; Hasegawa, J.; Ishida, M.; Nakajima, T.; Honda, Y.; Kitao, O.; Nakai, H.; Vreven, T.; Throssell, K.; Montgomery Jr, J. A.; Peralta, J. E.; Ogliaro, F.; Bearpark, M. J.; Heyd, J. J.; Brothers, E. N.; Kudin, K. N.; Staroverov, V. N.; Keith, T. A.; Kobayashi, R.; Normand, J.; Raghavachari, K.; Rendell, A. P.; Burant, J. C.; Iyengar, S. S.; Tomasi, J.; Cossi, M.; Millam, J. M.; Klene, M.; Adamo, C.; Cammi, R.; Ochterski, J. W.; Martin, R. L.; Morokuma, K.; Farkas, O.; Foresman, J. B.; Fox, D. J. Gaussian 16 Revision A.03. Wallingford, CT 2016.

(84) Perdew, J. P.; Burke, K.; Ernzerhof, M. Generalized Gradient Approximation Made Simple. *Phys. Rev. Lett.* **1996**, *77* (18), 3865–3868. https://doi.org/10.1103/PhysRevLett.77.3865.

(85) Adamo, C.; Barone, V. Toward Reliable Density Functional Methods without Adjustable Parameters: The PBE0 Model. *J. Chem. Phys.* **1999**, *110* (13), 6158–6170. https://doi.org/10.1063/1.478522.

(86) Alex D. Beck. Density-Functional Thermochemistry. III. The Role of Exact Exchange. *J. Chem. Phys.* **1993**, *98* (7), 5648–5656.

(87) Lee, C.; Yang, W.; Parr, R. G. Development of the Colle-Salvetti Correlation-Energy Formula into a Functional of the Electron Density. *Phys. Rev. B* **1988**, *37* (2), 785–789. https://doi.org/10.1103/PhysRevB.37.785.

(88) Stephen, P. J.; Devlin, F. J.; Chabalowski, C. F.; Frisch, M. J. Ab Initio Calculation of Vibrational Absorption and Circular Dichroism Spectra Using Density Functional Force Fields. *J. Phys. Chem.* **1994**, *98* (45), 11623–11627.

(89) Yanai, T.; Tew, D. P.; Handy, N. C. A New Hybrid Exchange-Correlation Functional Using the Coulomb-Attenuating Method (CAM-B3LYP). *Chem. Phys. Lett.* **2004**, *393* (1–3), 51–57. https://doi.org/10.1016/j.cplett.2004.06.011.

(90) Grimme, S.; Ehrlich, S.; Goerigk, L. Effect of the Damping Function in Dispersion Corrected Density Functional Theory. *J. Comput. Chem.* **2011**, *32* (7), 1456–1465. https://doi.org/https://doi.org/10.1002/jcc.21759.

(91) Grimme, S.; Antony, J.; Ehrlich, S.; Krieg, H. A Consistent and Accurate Ab Initio Parametrization of Density Functional Dispersion Correction (DFT-D) for the 94 Elements H-Pu. *J. Chem. Phys.* **2010**, *132* (15). https://doi.org/10.1063/1.3382344.

(92) Møller, C.; Plesset, M. S. Note on an Approximation Treatment for Many-Electron Systems. *Phys. Rev.* **1934**, *46* (7), 618–622. https://doi.org/10.1103/PhysRev.46.618.

(93) Krishnan, R.; Binkley, J. S.; Seeger, R.; Pople, J. A. Self-Consistent Molecular Orbital Methods. XX. A Basis Set for Correlated Wave Functions. *J. Chem. Phys.* **1980**, *72* (1), 650–654. https://doi.org/10.1063/1.438955.

(94) Clark, T.; Chandrasekhar, J.; Spitznagel, G. W.; Schleyer, P. V. R. Efficient Diffuse Function-Augmented Basis Sets for Anion Calculations. III. The 3-21+G Basis Set for First-Row Elements, Li–F. *J. Comput. Chem.* **1983**, *4* (3), 294–301. https://doi.org/https://doi.org/10.1002/jcc.540040303.

(95) Weigend, F. Accurate Coulomb-Fitting Basis Sets for H to Rn. *Phys. Chem. Chem. Phys.* **2006**, *8* (9), 1057–1065. https://doi.org/10.1039/b515623h.

(96) Weigend, F.; Ahlrichs, R. Balanced Basis Sets of Split Valence, Triple Zeta Valence and Quadruple Zeta Valence Quality for H to Rn: Design and Assessment of Accuracy. *Phys. Chem. Chem. Phys.* **2005**, *7* (18), 3297–3305. https://doi.org/10.1039/b508541a.

(97) Bruce, M. I.; Zwar, J. A. Cytokinin Activity of Some Substituted Ureas and Thioureas. *Proc. R. Soc. London. Ser. B, Contain. Pap. a Biol. character. R. Soc. (Great Britain)* **1966**, *165* (999), 245–265. https://doi.org/10.1098/rspb.1966.0067.

(98) Tjernberg, A.; Markova, N.; Griffiths, W. J.; Hallén, D. DMSO-Related Effects in Protein Characterization. *J. Biomol. Screen.* **2006**, *11* (2), 131–137. https://doi.org/10.1177/1087057105284218.

(99) Sivasakthi, V.; Anbarasu, A.; Ramaiah, S. π-π Interactions in Structural Stability: Role in RNA Binding Proteins. *Cell Biochem. Biophys.* **2013**, *67* (3), 853–863. https://doi.org/10.1007/s12013-013-9573-0.

(100) Ly, T.; Julian, R. R. Using ESI-MS to Probe Protein Structure by Site-Specific Noncovalent Attachment of 18-Crown-6. J. Am. Soc. Mass Spectrom. 2006, 17 (9), 1209–1215. https://doi.org/10.1016/j.jasms.2006.05.007.

(101) Rüütel, A.; Tshepelevitsh, S.; Leito, I. One Hundred Carboxylate Receptors. J. Org. Chem. **2022.** https://doi.org/10.1021/acs.joc.2c01725.

(102) Hamdy, O. M.; Julian, R. R. Reflections on Charge State Distributions, Protein Structure, and the Mystical Mechanism of Electrospray Ionization. J. Am. Soc. Mass Spectrom. 2012, 23 (1), 1–6. https://doi.org/10.1007/s13361-011-0284-8

Supplementary Information for Diserinol Isophthalamide: A Novel Reagent for Complexation with Biomolecular Anions in Electrospray Ionization Mass Spectrometry

Madeline Schultz, Sarah L. Parker, Maleesha T. Fernando, Miyuru M. Wellalage, Daniel A. Thomas*

Department of Chemistry, University of Rhode Island, Kingston, RI, 02881, USA
Email: dathomas@uri.edu

Table of Contents

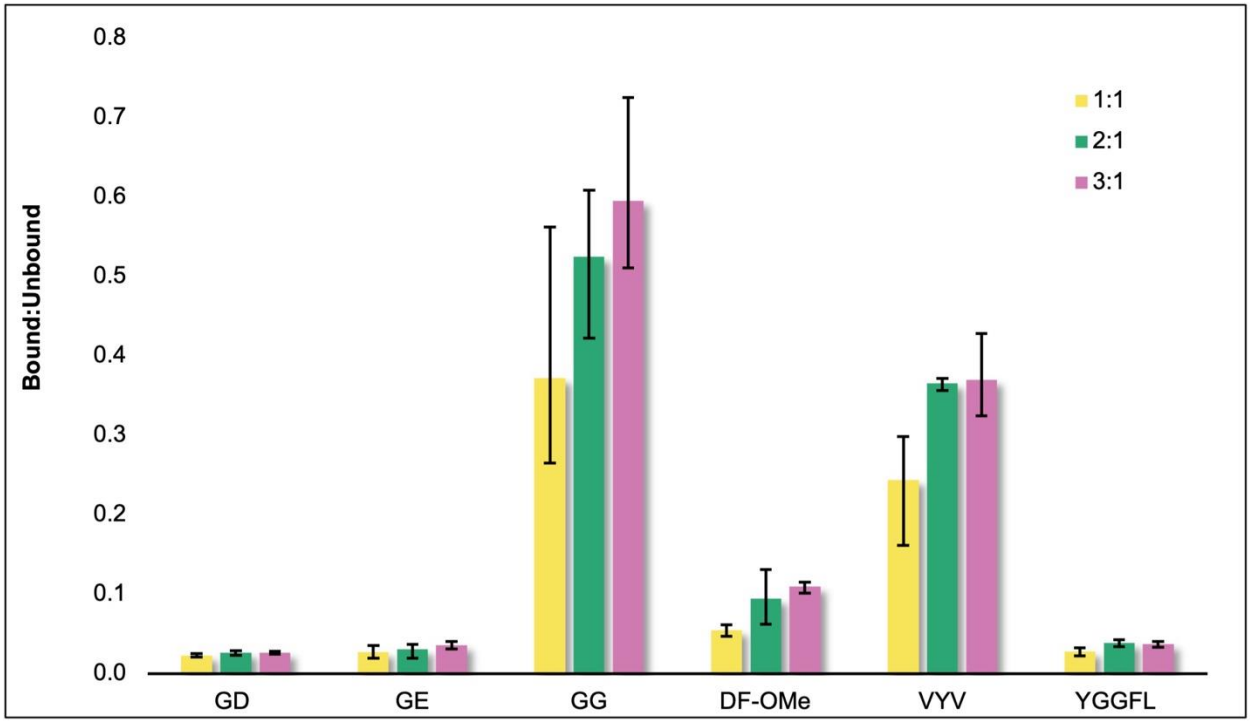

Figure S1. The ratio of bound complex to unbound free peptide is shown for PBP/peptide spectra. Concentration of peptide was 10 μM and the concentration of PBP was varied: 10 μM (yellow), 20 μM (green) and 30 μM (pink) respectively. Error bars show the high/low values from three samples.

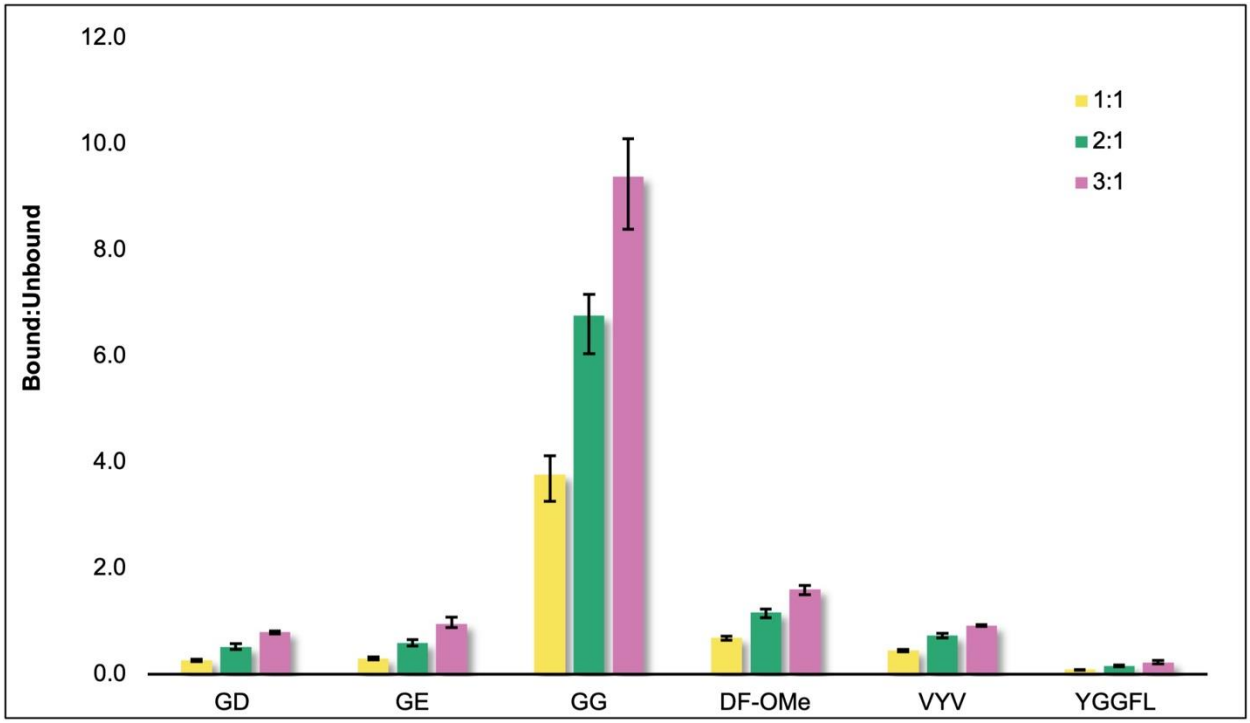

Figure S2. The ratio of bound complex to unbound free peptide is shown for DIP/peptide spectra. Concentration of peptide was 10 μM and the concentration of DIP was varied: 10 μM (yellow), 20 μM (green) and 30 μM (pink) respectively. Error bars show the high/low values from three samples.

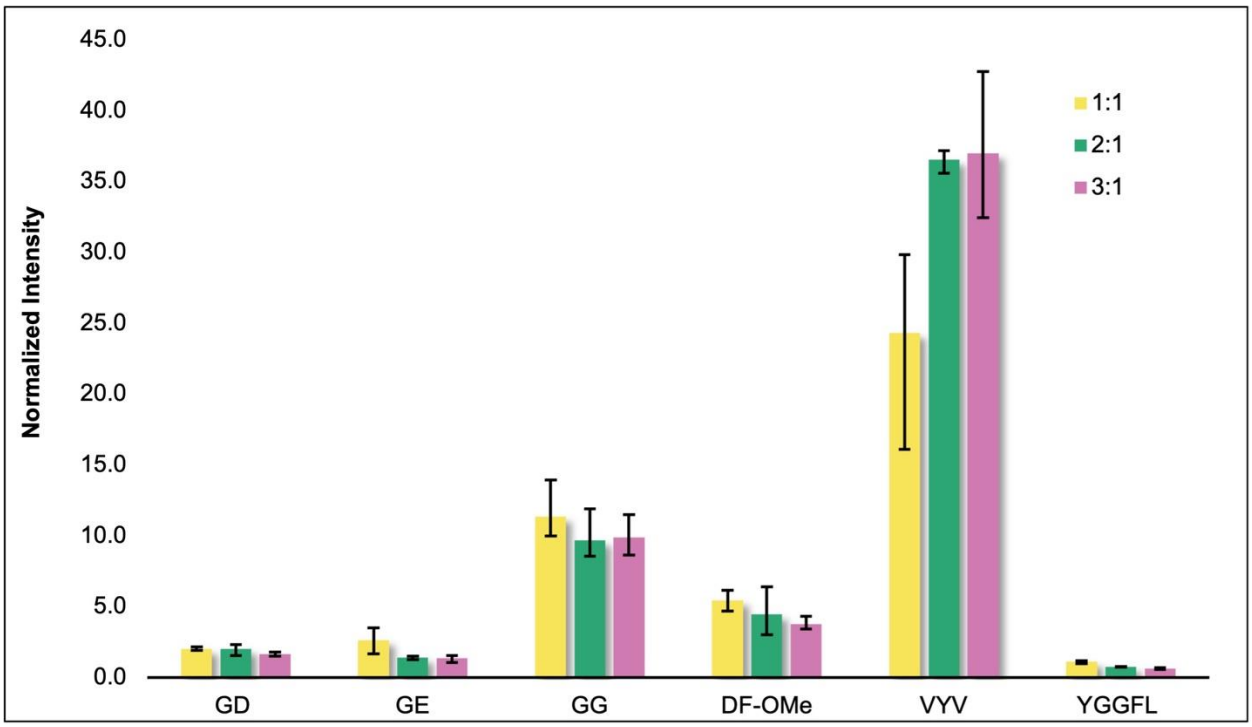

Figure S3. The normalized intensity of complexed species is shown for PBP/peptide spectra. Concentration of peptide was 10 μM and the concentration of PBP was varied: 10 μM (yellow), 20 μM (green) and 30 μM (pink) respectively. Error bars show the high/low values from three samples.

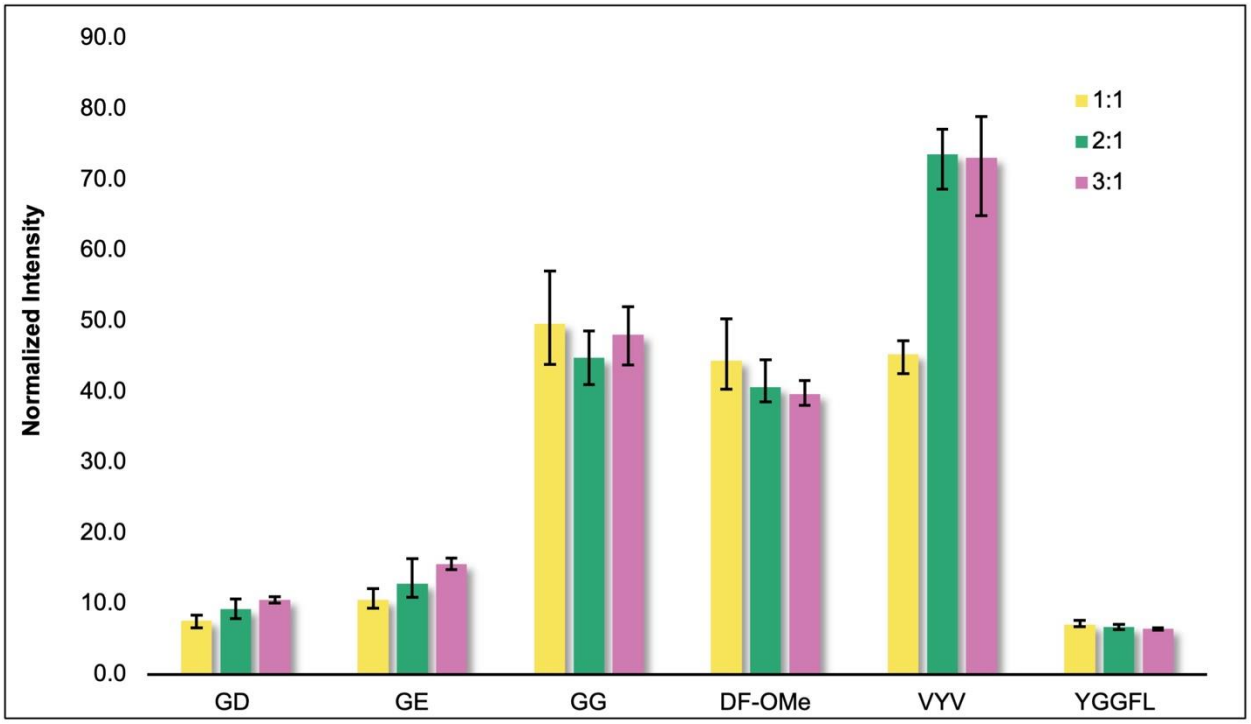

Figure S4. The normalized intensity of complexed species is shown for DIP/peptide spectra. Concentration of peptide was 10 μM and the concentration of DIP was varied: 10 μM (yellow), 20 μM (green) and 30 μM (pink) respectively. Error bars show the high/low values from three samples.

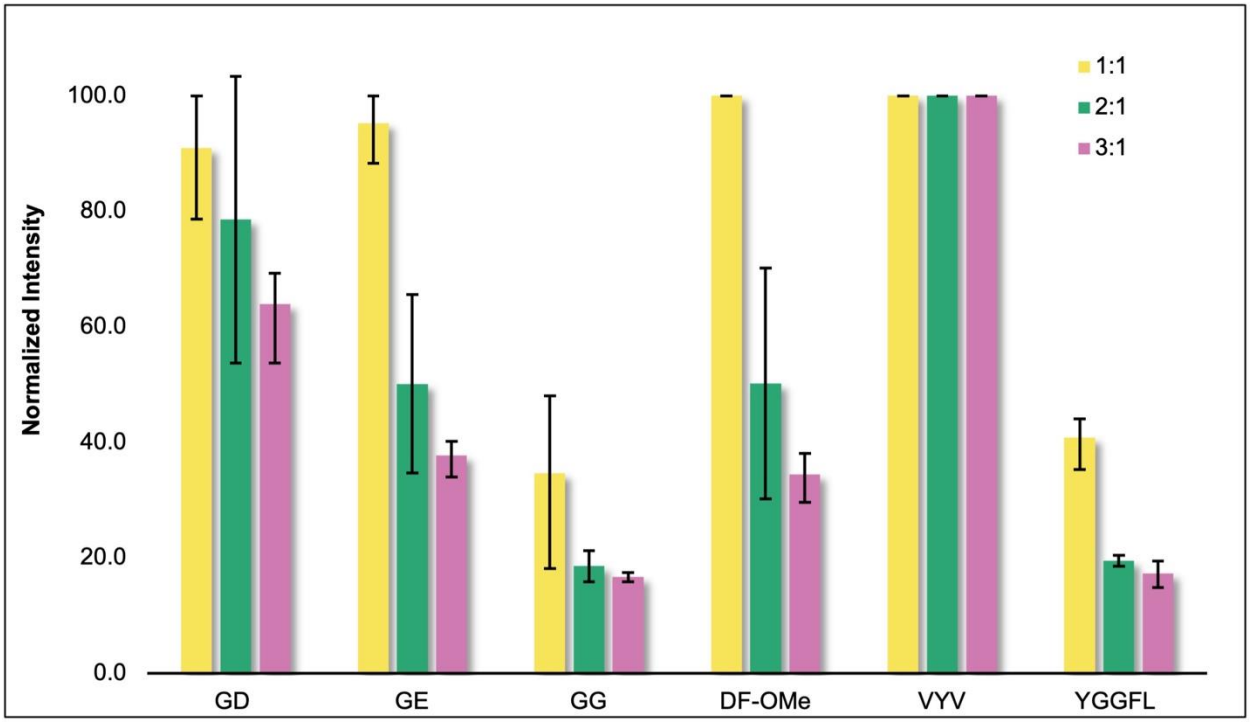

Figure S5. The normalized intensity of free peptide is shown for PBP/peptide spectra. Concentration of peptide was 10 μM and the concentration of PBP was varied: 10 μM (yellow), 20 μM (green) and 30 μM (pink) respectively. Error bars show the high/low values from three samples.

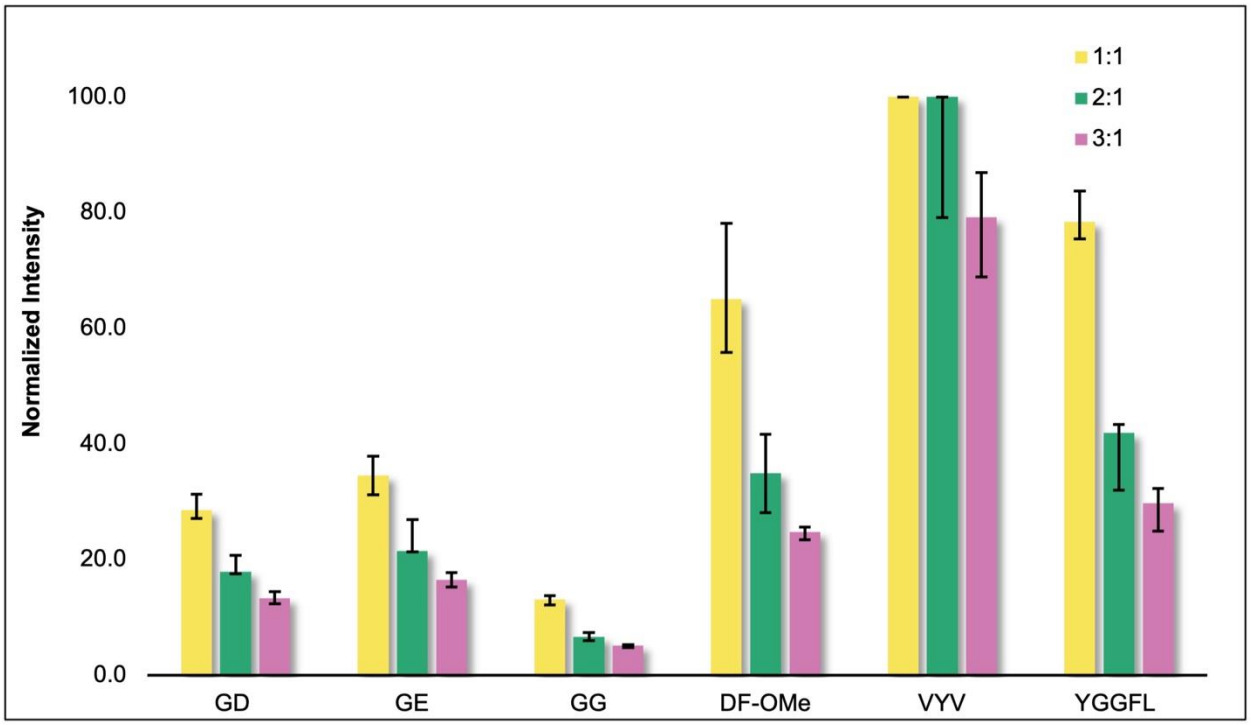

Figure S6. The normalized intensity of free peptide is shown for DIP/peptide spectra. Concentration of peptide was 10 μM and the concentration of DIP was varied: 10 μM (yellow), 20 μM (green) and 30 μM (pink) respectively. Error bars show the high/low values from three samples.

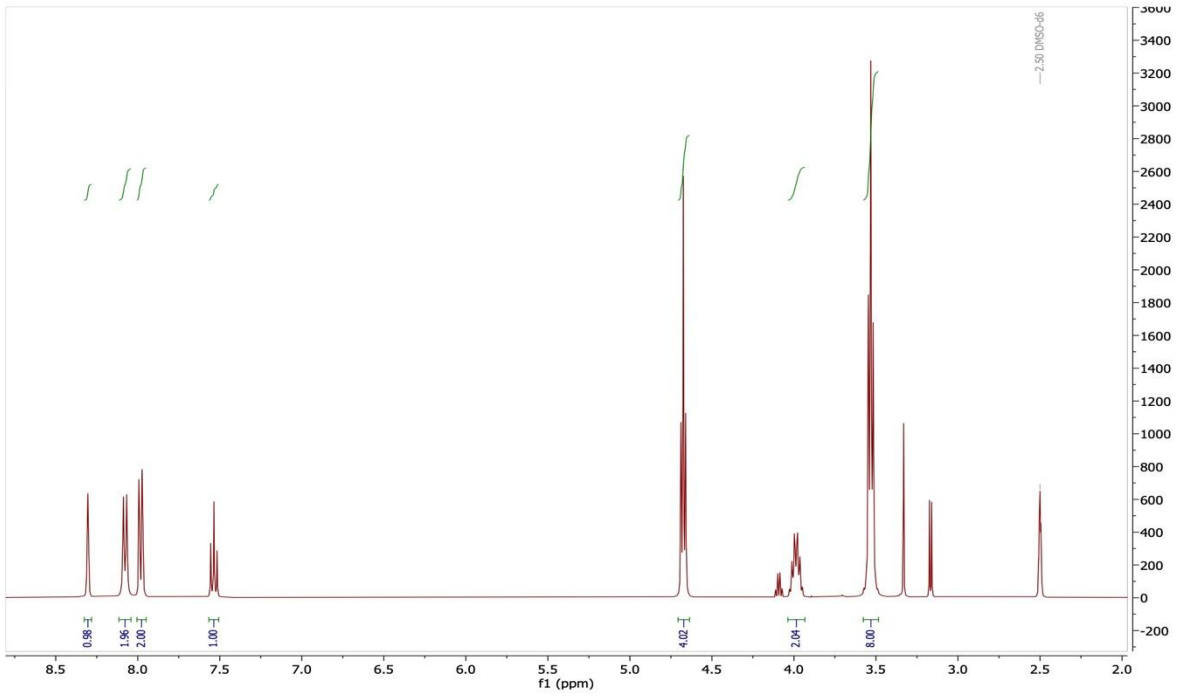

Figure S7. ^{1}H NMR spectrum of DIP.

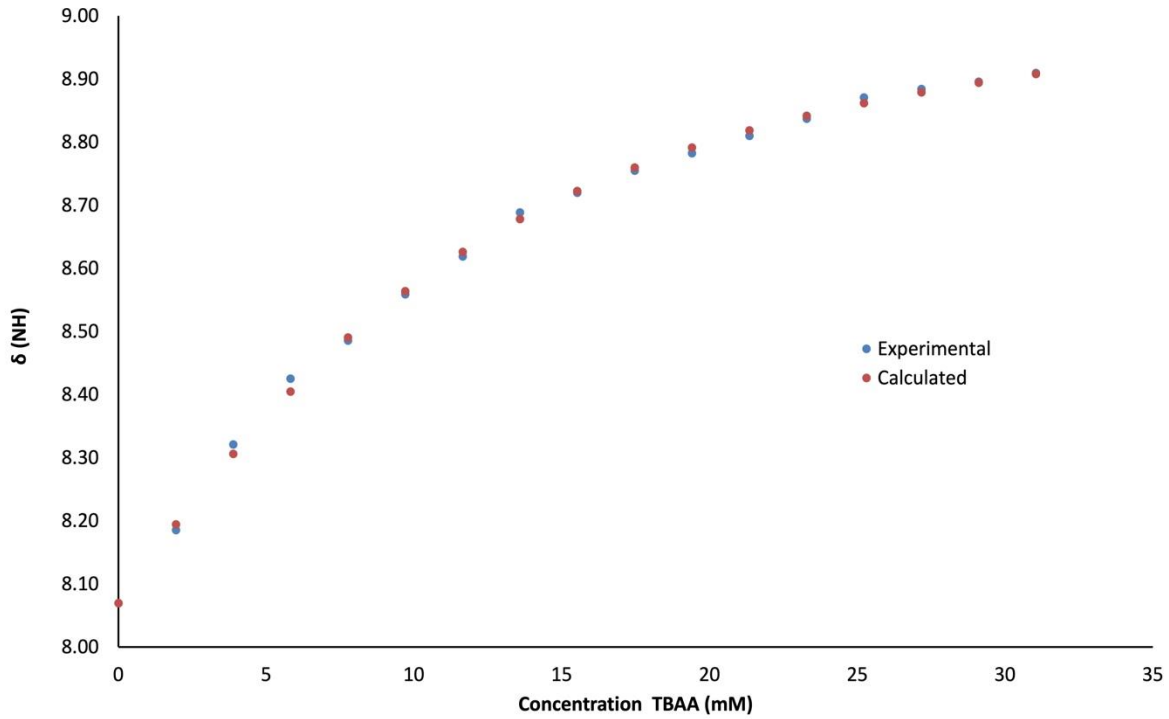

Figure S8. ^{1}H NMR titration curve for DIP (10mM) with varied concentration of TBAA. Analysis was performed in duplicate.

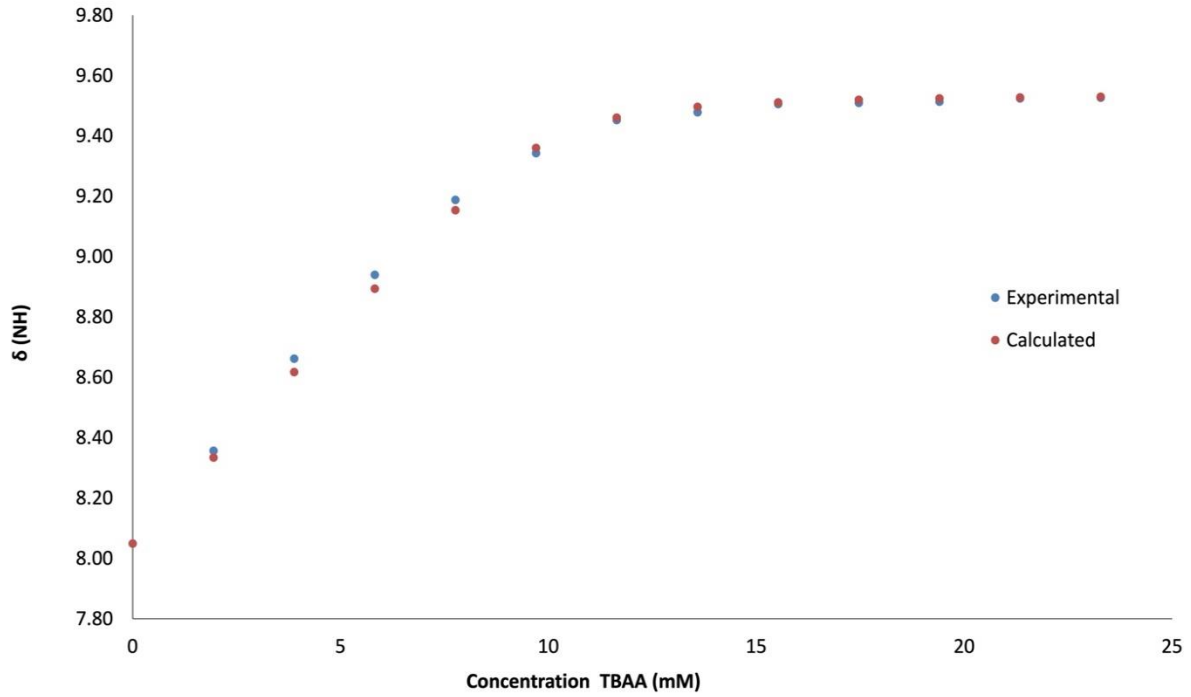

Figure S9. ^{1}H NMR titration curve for PBP (10mM) with varied concentration of TBAA. Analysis was performed in duplicate

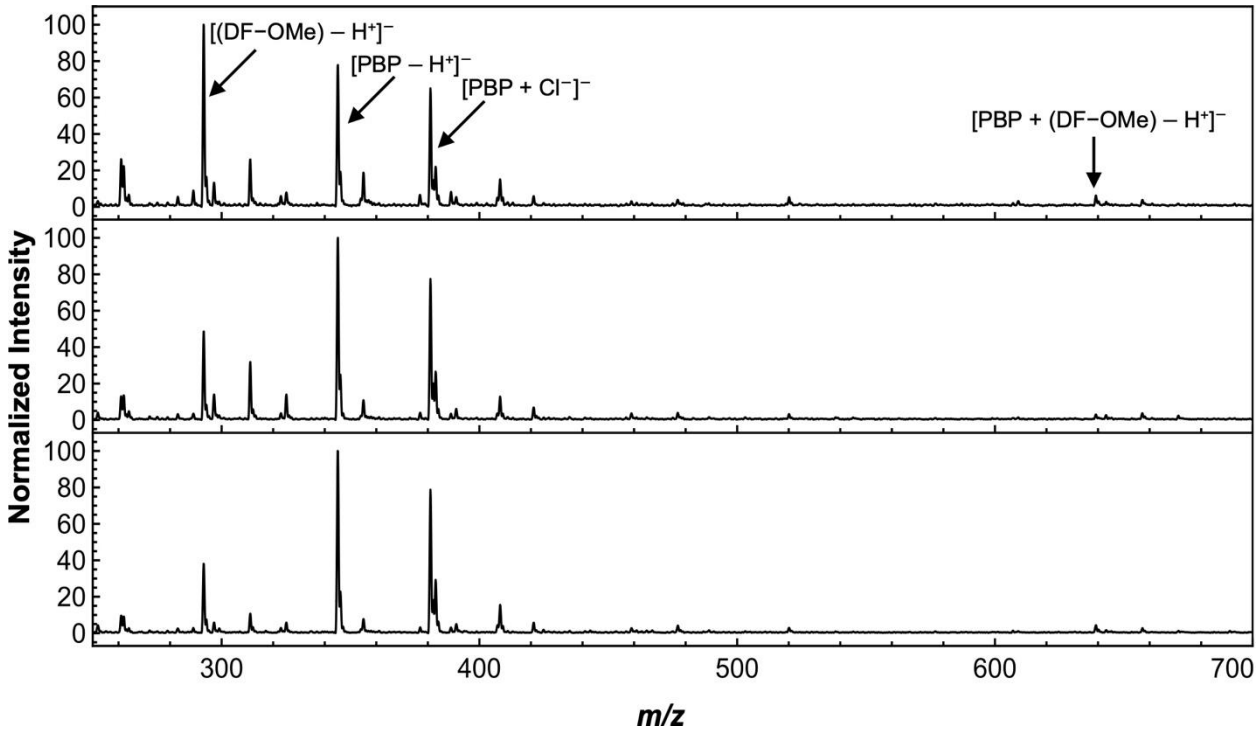

Figure S10. Mass spectra for PBP: DF-OMe in 80/20 H_2O/MeOH at varied concentrations of reagent to peptide: 10:10 μM (top), 20:10 μM (middle) and 30:10 μM (bottom).

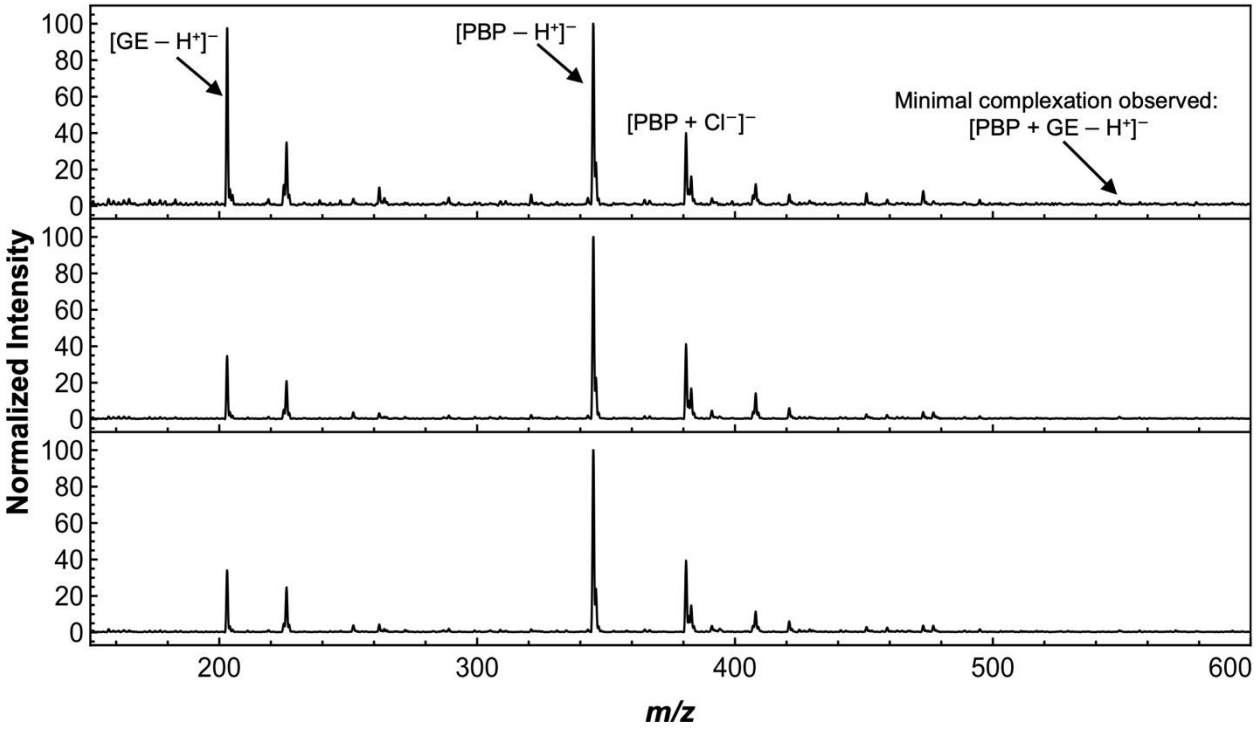

Figure S11. Mass spectra for PBP: GE in 80/20 H_2O/MeOH at varied concentrations of reagent to peptide: 10:10 μM (top), 20:10 μM (middle) and 30:10 μM (bottom).

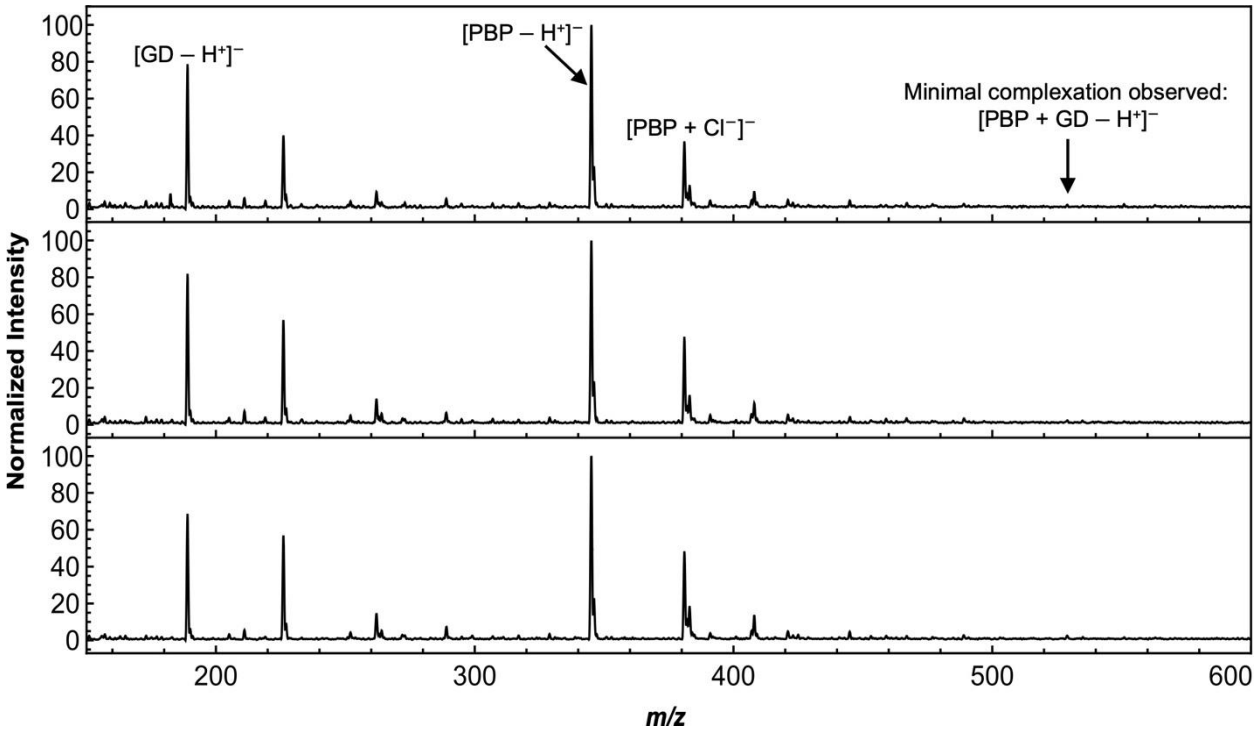

Figure S12. Mass spectra for PBP: GD in 80/20 H_2O/MeOH at varied concentrations of reagent to peptide: 10:10 μM (top), 20:10 μM (middle) and 30:10 μM (bottom).

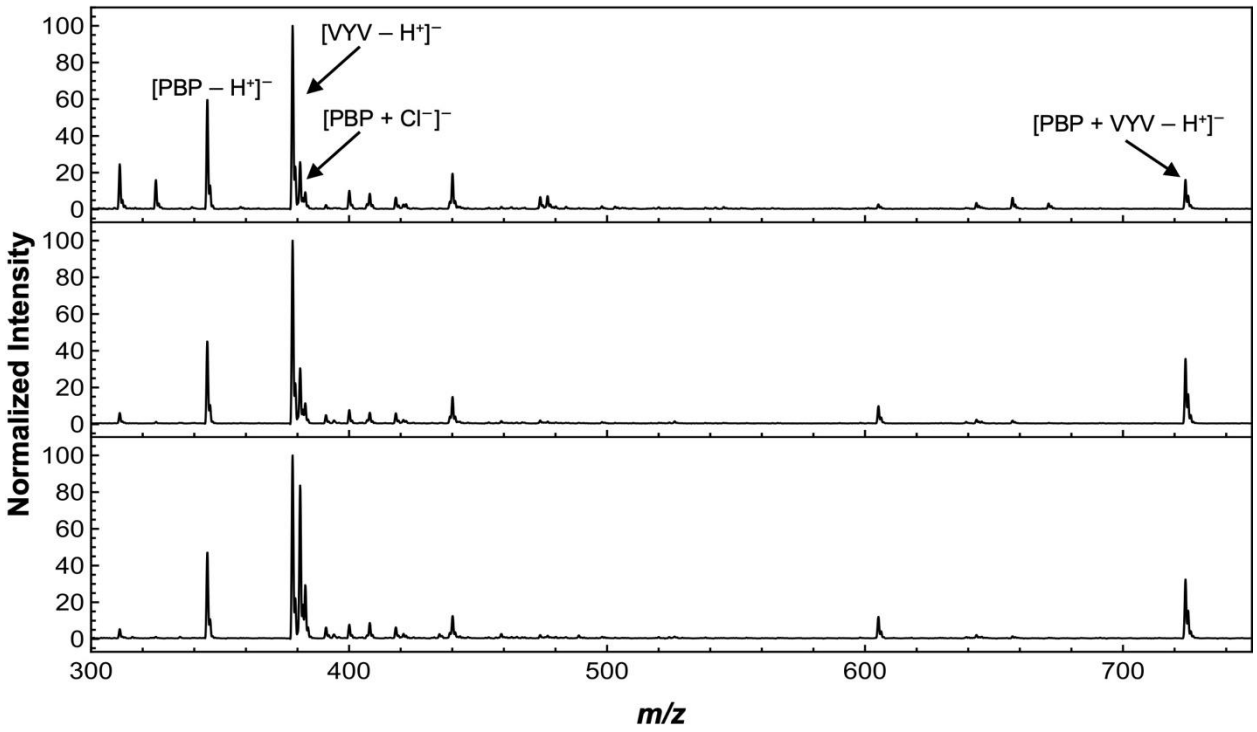

Figure S13. Mass spectra for PBP:VYV in 80/20 H_2O/MeOH at varied concentrations of reagent to peptide: 10:10 μM (top), 20:10 μM (middle) and 30:10 μM (bottom).

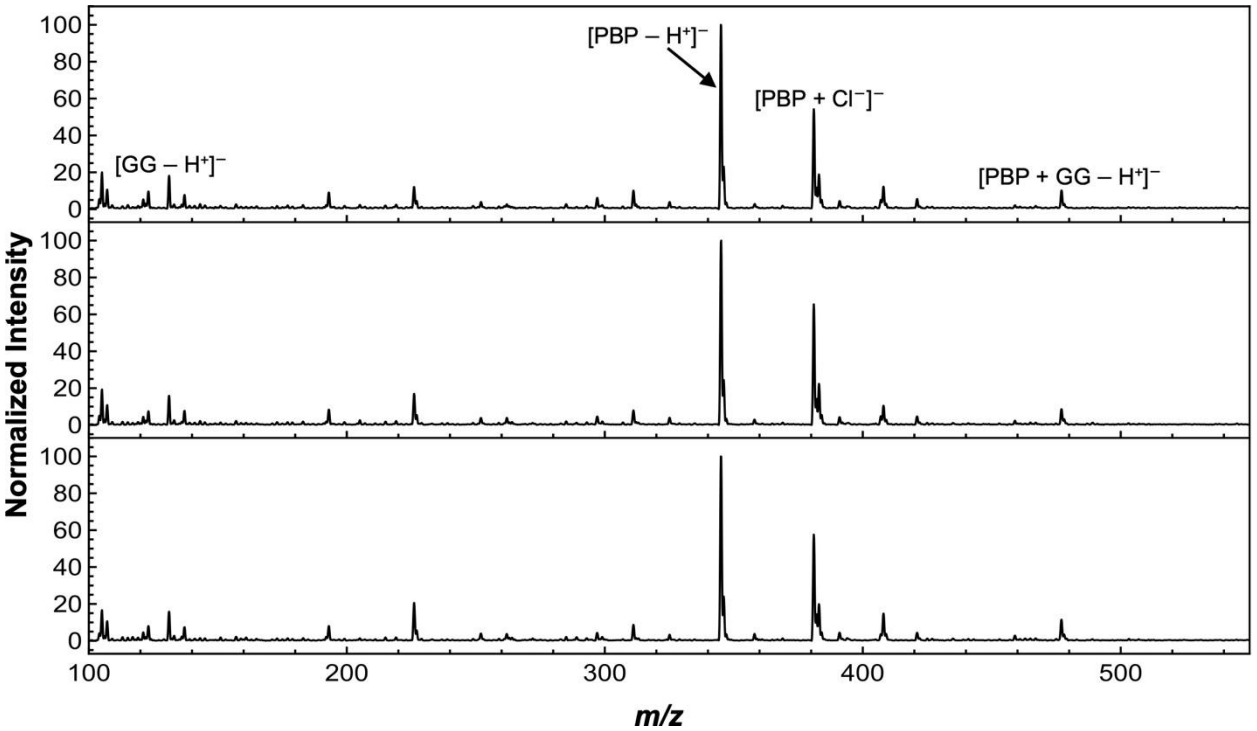

Figure S14. Mass spectra for PBP:GG in 80/20 H_2O/MeOH at varied concentrations of reagent to peptide: 10:10 μM (top), 20:10 μM (middle) and 30:10 μM (bottom).

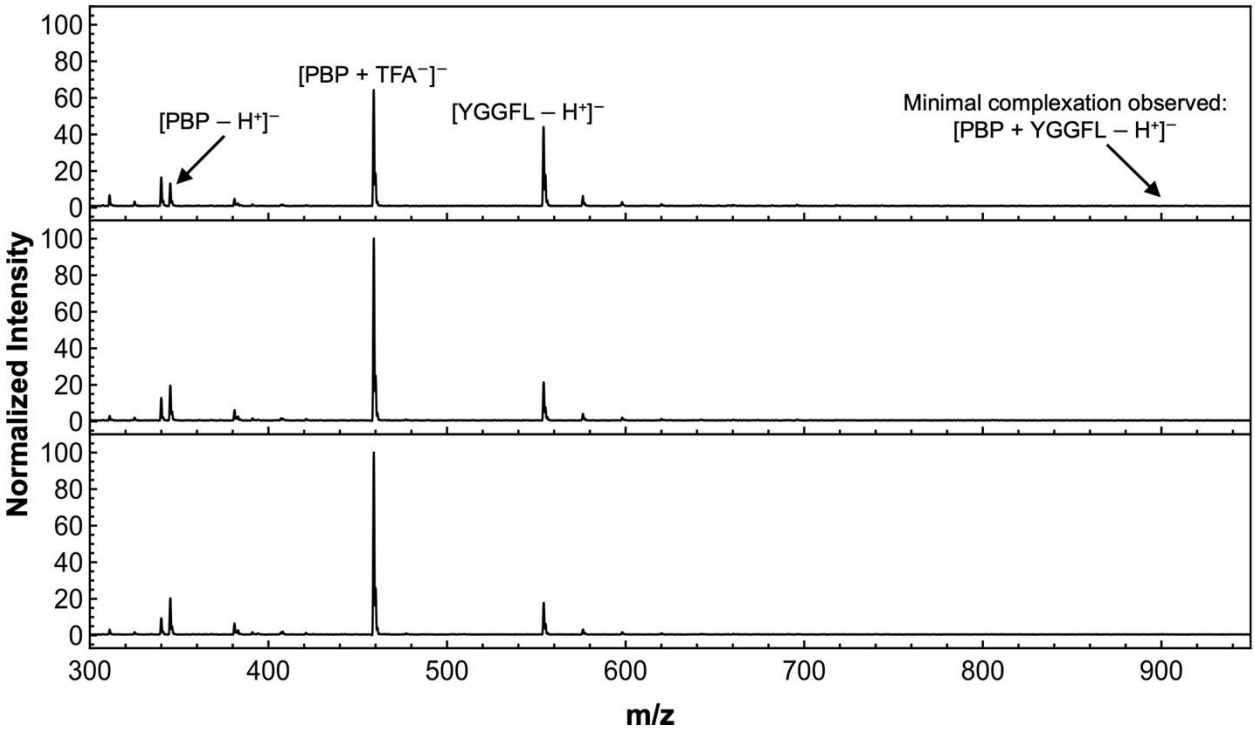

Figure S15. Mass spectra for PBP: YGGFL in 80/20 H_2O/MeOH at varied concentrations of reagent to peptide: 10:10 μM (top), 20:10 μM (middle) and 30:10 μM (bottom).

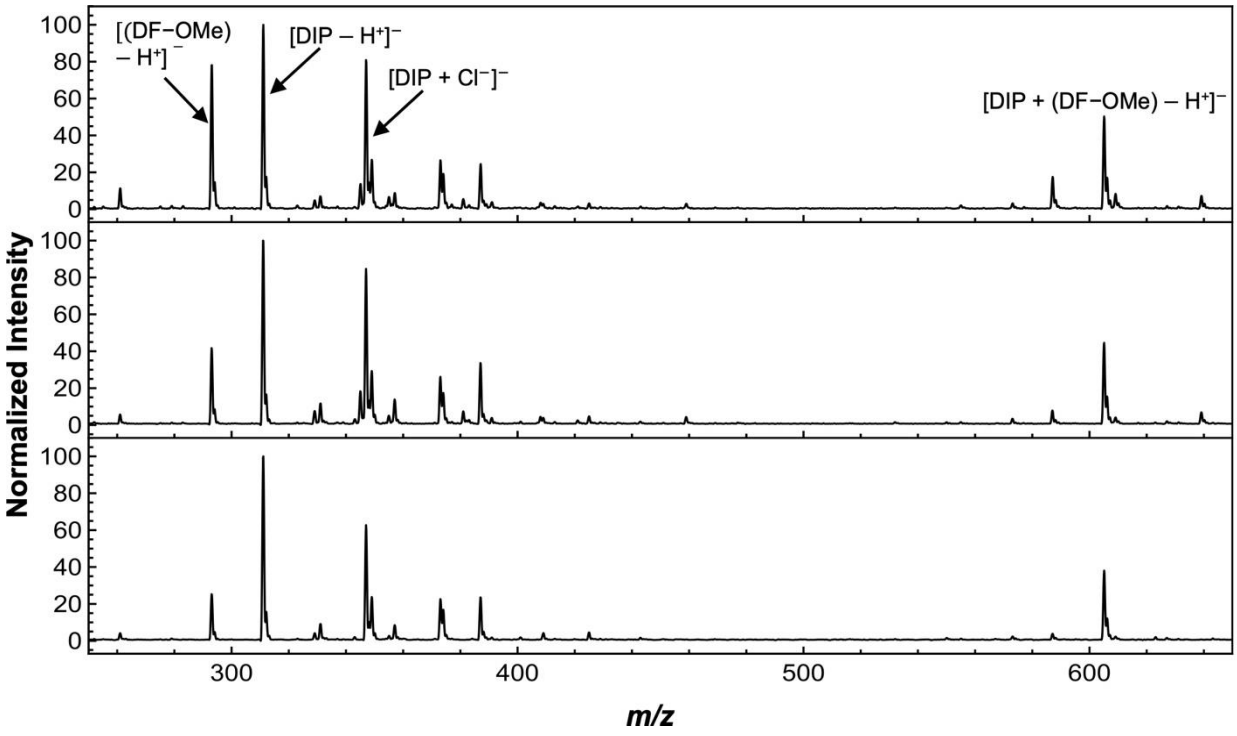

Figure S16. Mass spectra for DIP: DF-OMe in 80/20 H_2O/MeOH at varied concentrations of reagent to peptide: 10:10 μM (top), 20:10 μM (middle) and 30:10 μM (bottom).

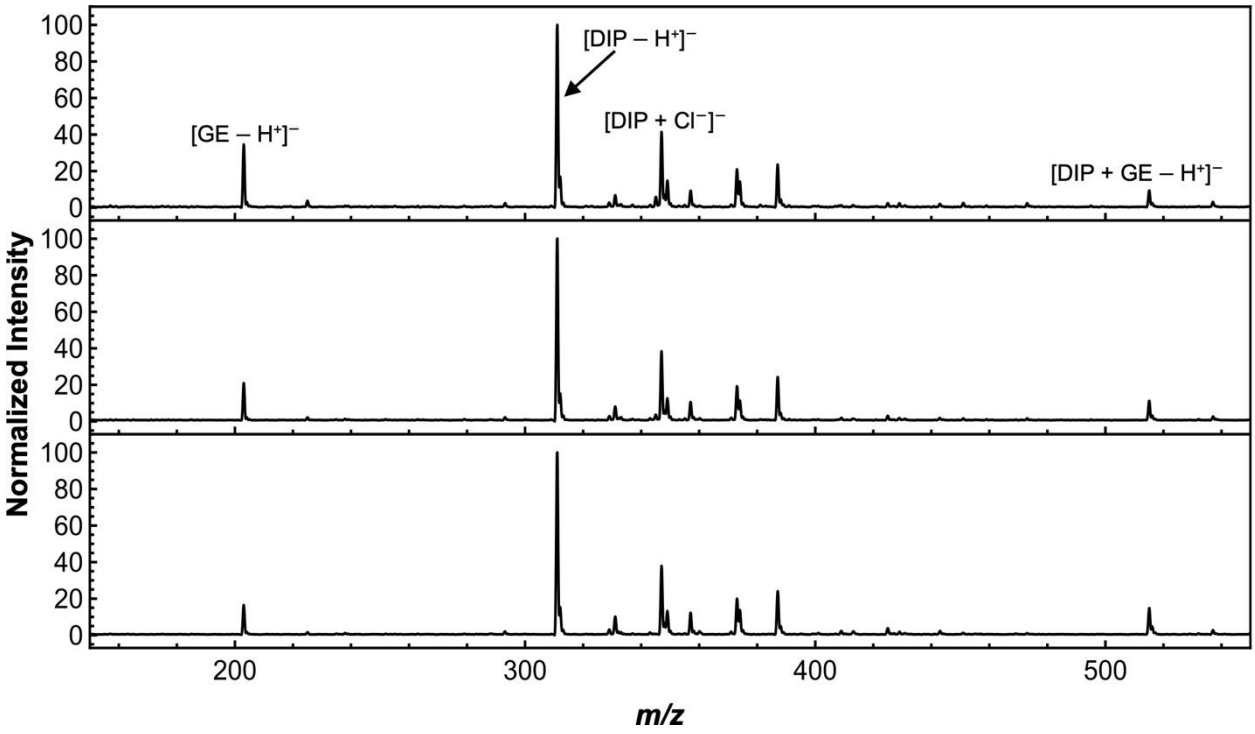

Figure S17. Mass spectra for DIP: GE in 80/20 H_2O/MeOH at varied concentrations of reagent to peptide: 10:10 μM (top), 20:10 μM (middle) and 30:10 μM (bottom).

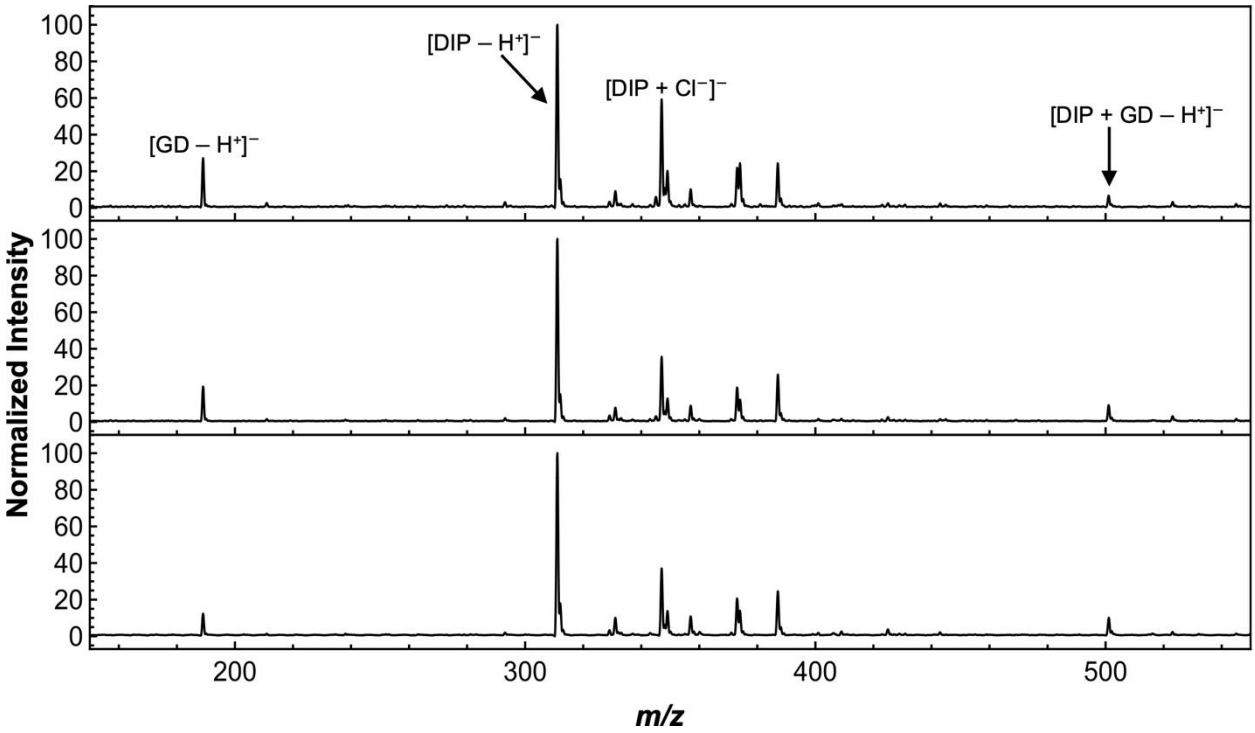

Figure S18. Mass spectra for DIP: GD in 80/20 H_2O/MeOH at varied concentrations of reagent to peptide: 10:10 μM (top), 20:10 μM (middle) and 30:10 μM (bottom).

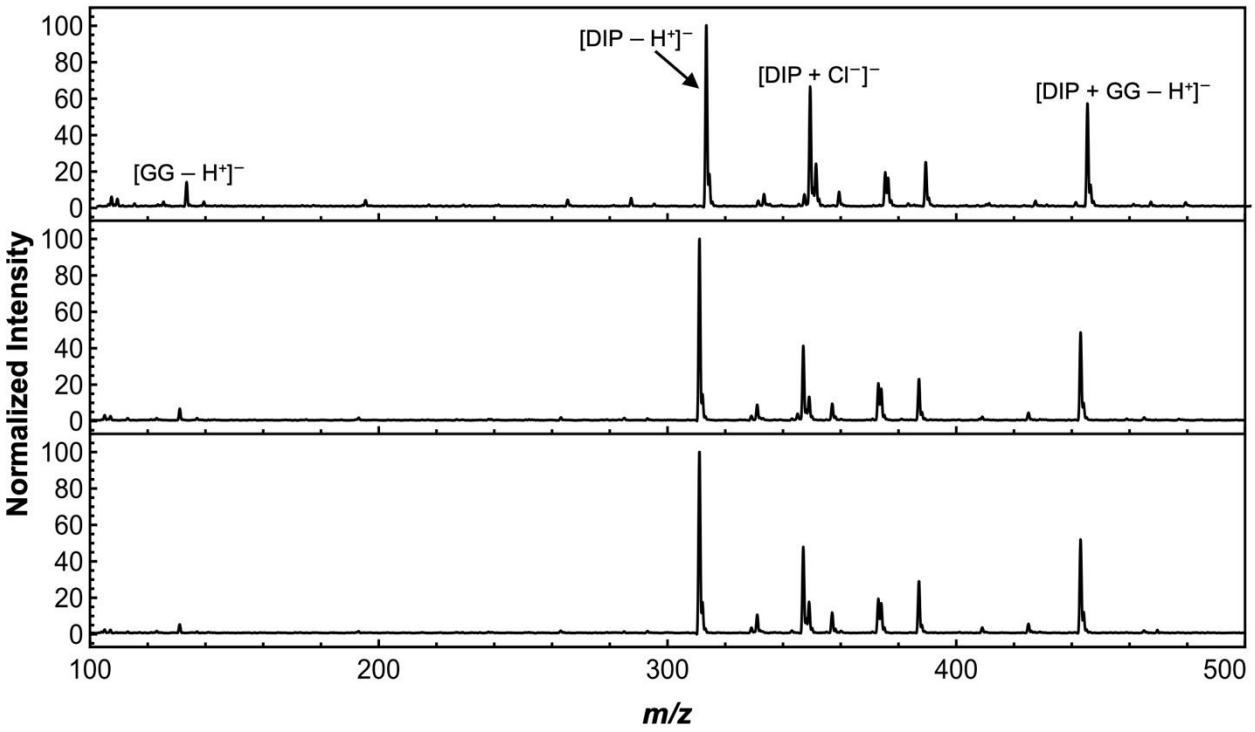

Figure S19. Mass spectra for DIP: GG in 80/20 H_2O/MeOH at varied concentrations of reagent to peptide: 10:10 μM (top), 20:10 μM (middle) and 30:10 μM (bottom).

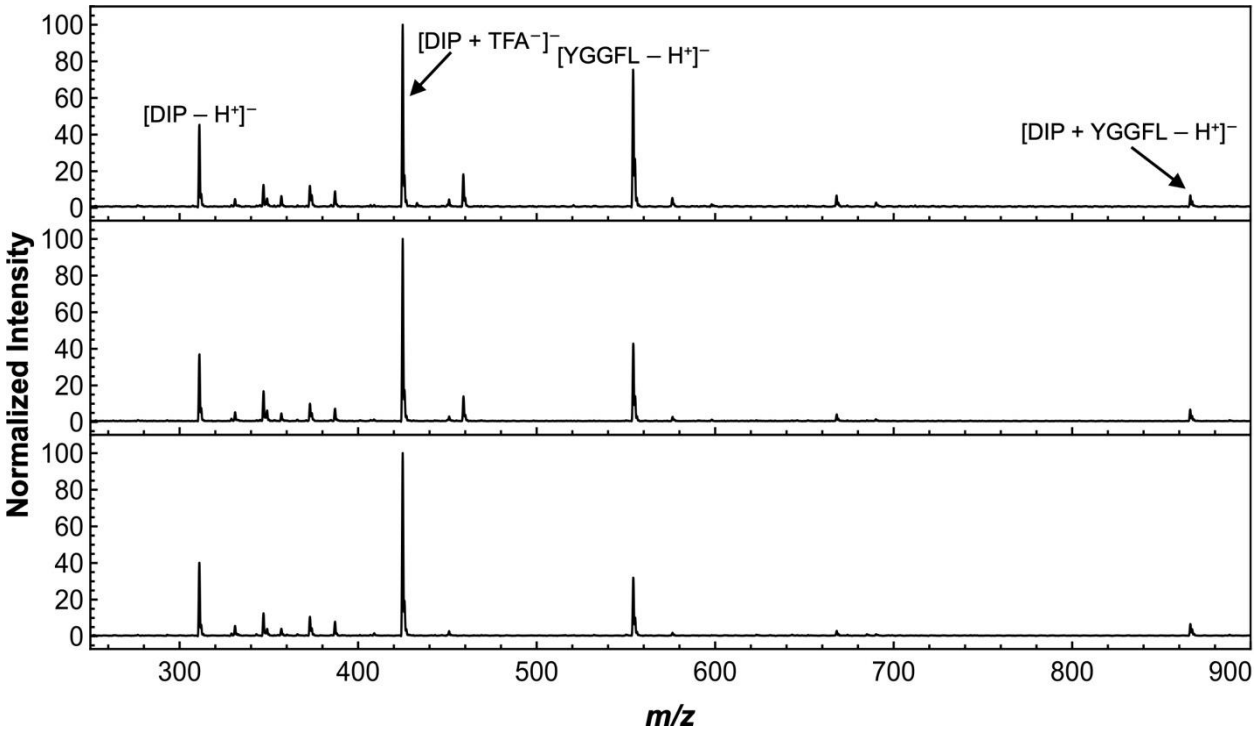

Figure S20. Mass spectra for DIP: YGGFL in 80/20 H_2O/MeOH at varied concentrations of reagent to peptide: 10:10 μM (top), 20:10 μM (middle) and 30:10 μM (bottom).

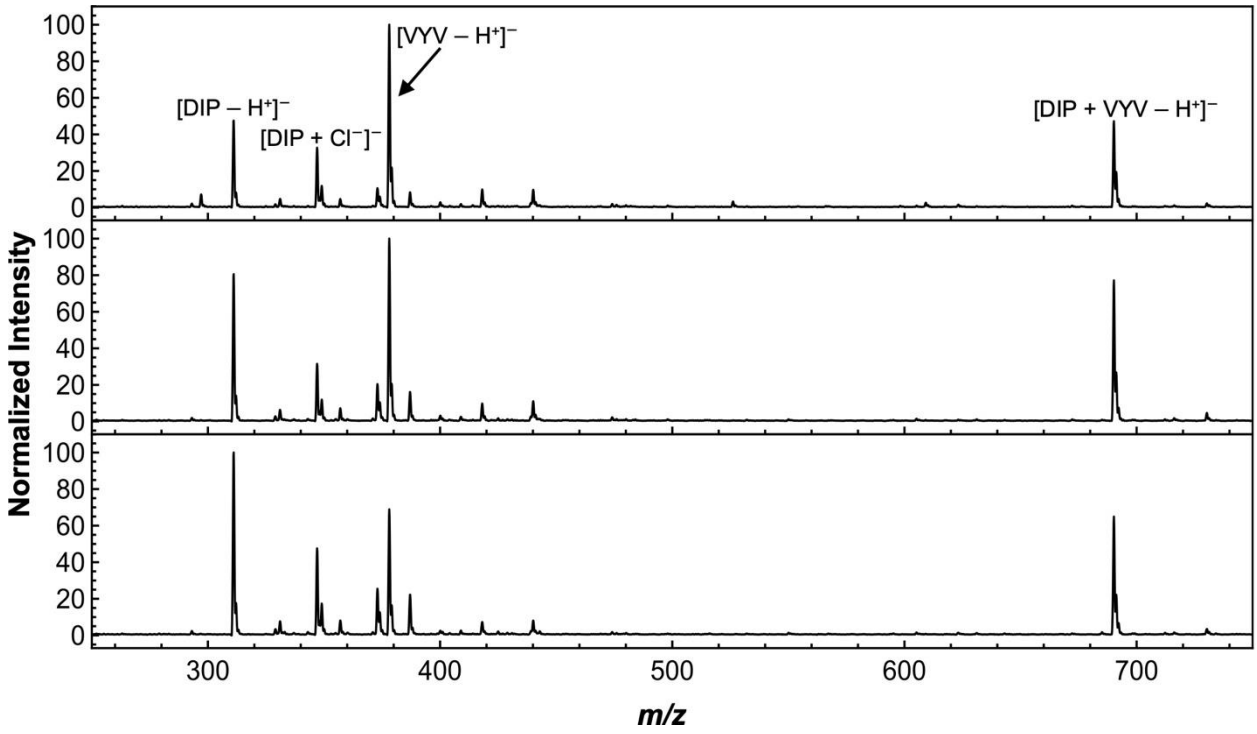

Figure S21. Mass spectra for DIP: VYV in 80/20 H_2O/MeOH at varied concentrations of reagent to peptide: 10:10 μM (top), 20:10 μM (middle) and 30:10 μM (bottom).

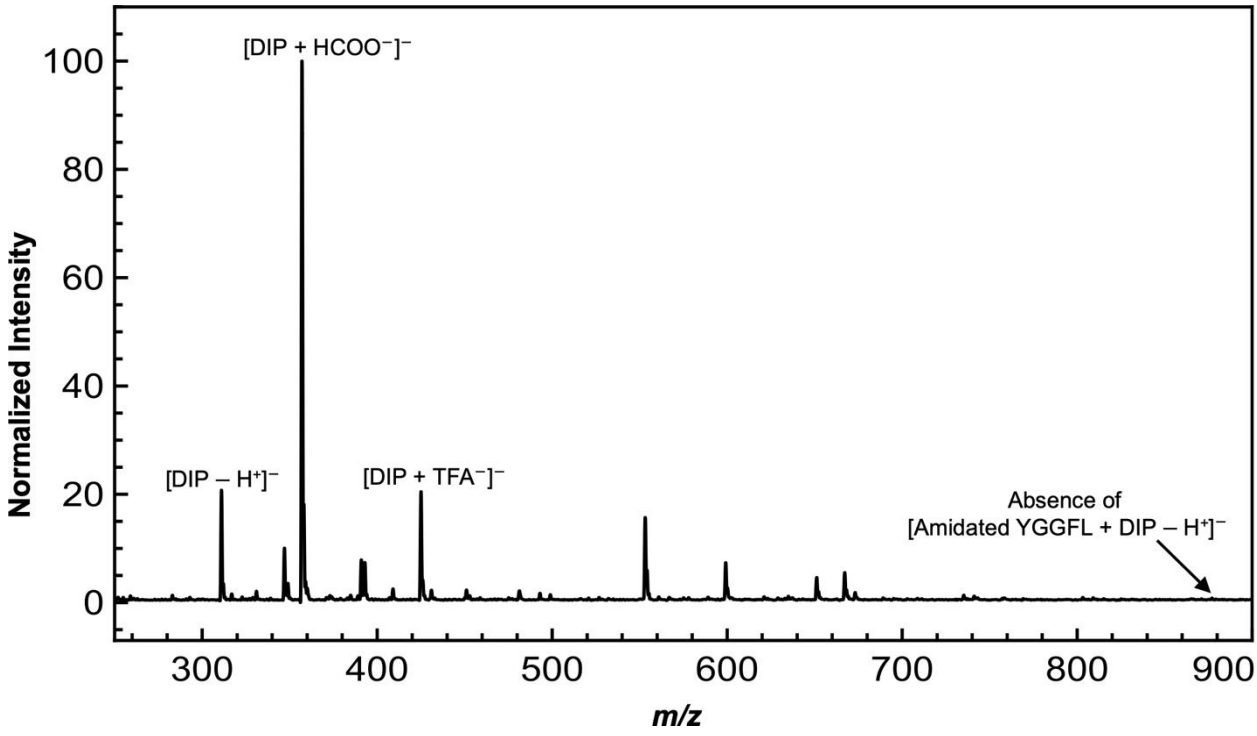

Figure S22. Mass spectrum of DIP: amidated YGGFL (30: 10 μM) in MeOH/H_2O (80/20 v/v%).

Table S1. Computed Electronic Energies of PBP and DIP Complexes with Acetate.[a]

Structure	MP2/ 6-311++G(d, p)	PBE0(D3BJ)/ 6-311++G(d, p)	PBE0(D3BJ)/def2-TZVPP	B3LYP(D3BJ)/6-311++G(d, p)	CAM-B3LYP(D3BJ)/6-311++G(d, p)
1	-1331.848901562	-1333.9731353	-1334.120988	-1335.52573257	-1334.89540998
2	-1331.8490590768	N/A	N/A	N/A	N/A
3	N/A	-1369.96145875	N/A	-1371.59621249	-1370.86923842
4	-1367.6377608205	N/A	-1370.11876356	N/A	N/A

a. values reported in Hartrees.